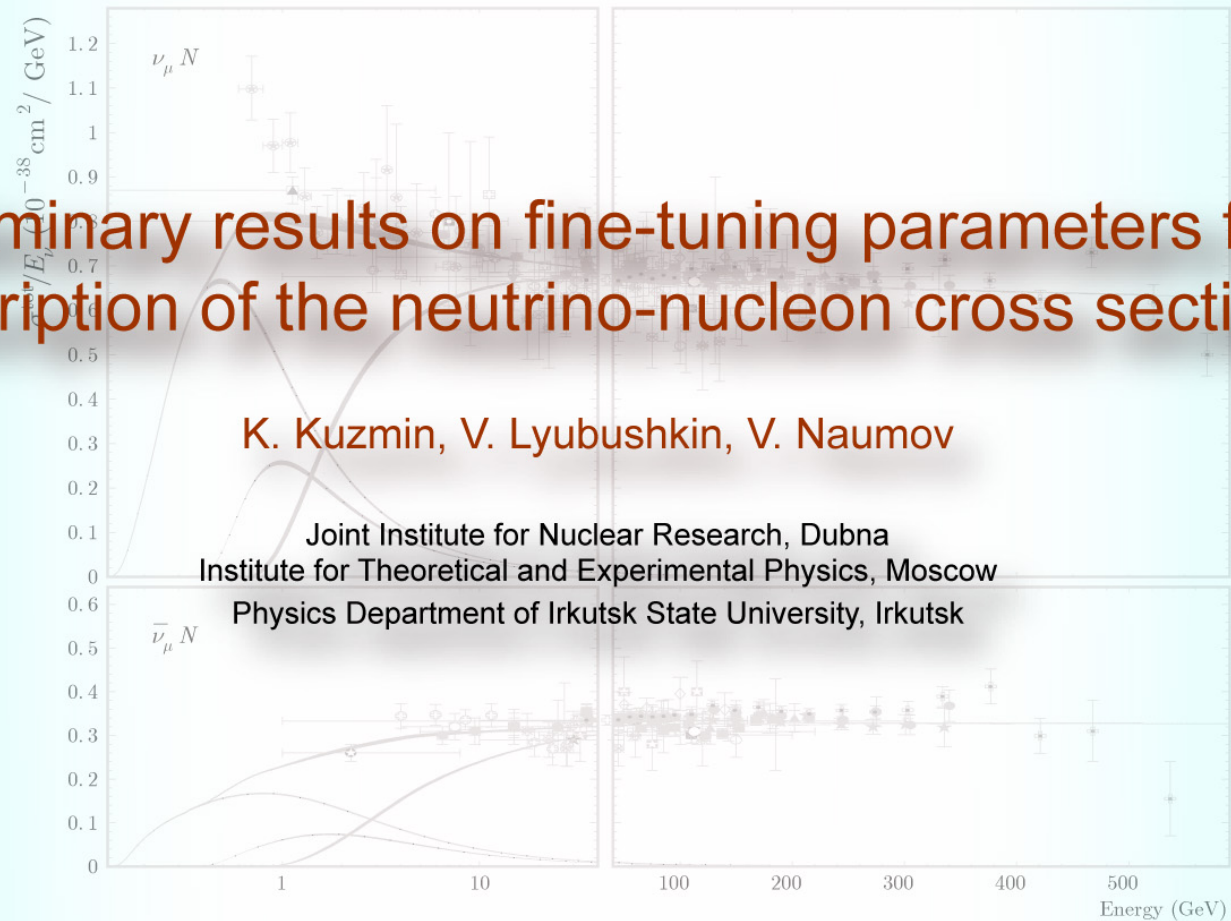


# Preliminary results on fine-tuning parameters for description of the neutrino-nucleon cross sections

K. Kuzmin, V. Lyubushkin, V. Naumov

Joint Institute for Nuclear Research, Dubna  
Institute for Theoretical and Experimental Physics, Moscow

Physics Department of Irkutsk State University, Irkutsk



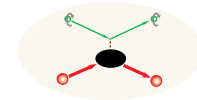
# Plan of the talk

1. Introduction (aims & scopes)

---

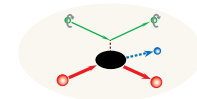
2. Quasielastic scattering [QES]

---



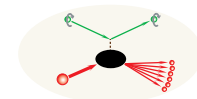
3. Single-pion production through baryon resonances [RES]

---



4. Deep inelastic scattering [DIS]

---



5. Global fit

---



6. (Instead of) summary

---

$$M_A^{\text{QES,RES}}$$
$$W_{\text{cut}}^{\text{RES,DIS}}$$

7. Additional matters

---



# INTRODUCTION: Aims & Scopes of **KL<sub>i</sub>N** Project

Our ultimate (and hardly attainable) aim is

An universal neutrino event generator for past, current, and future experiments with atmospheric and accelerator neutrinos for studying

- neutrino oscillations in vacuum and matter ( $\Delta m_{ij}$ ,  $\theta_{ij}$ , sterile  $\nu_s$ , quark-lepton complementarity, ...);
  - CP/T and Lorentz/CPT violation in the neutrino sector;
  - nonstandard neutrino interactions (2nd-class currents, flavor-changing NC, ...);
  - exotic phenomena (neutrino decay, quantum decoherence, flavor relaxation, ...);
- as well as for evaluating the atmospheric neutrino induced backgrounds to
- various astrophysical explorations (searches for cosmic neutrinos, relativistic neutralinos, mirror cosmic rays, ...);
  - searches for baryon number violation ( $p$  decay &  $n \leftrightarrow \bar{n}$  transitions in nuclei).

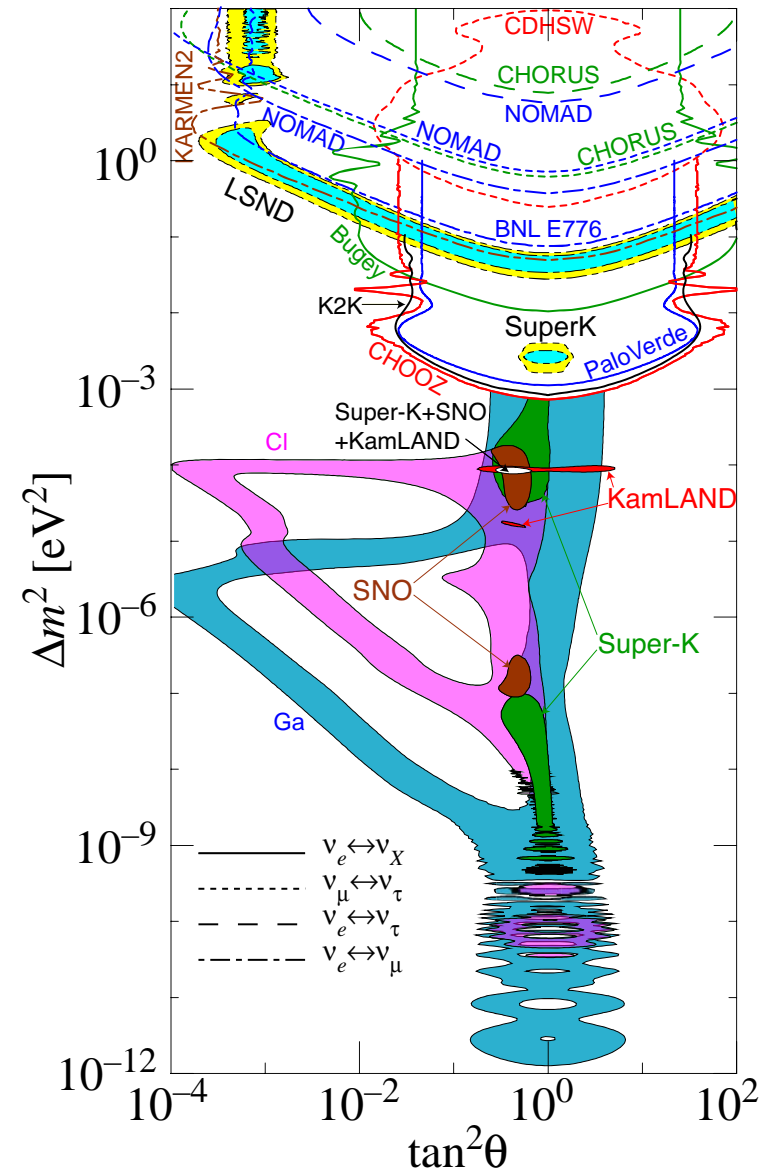


Good knowledge of neutrino-nucleon and neutrino-nucleus cross sections is a crucial imperative in the analyses of all these issues.

# Status of neutrino oscillation searches

The regions of neutrino squared-mass splitting and mixing angle favored or excluded by various experiments. Contributed to RPP-2006 [J. Phys. G **33** (2006) 1–1232] by Hitoshi Murayama (University of California, Berkeley).  
 [Borrowed from URL <http://hitoshi.berkeley.edu/>]

Figure shows the most rigorous current results and does not include the data from many earlier underground experiments (BUST, NUSEX, Fréjus, IMB, Kamiokande, MACRO, SOUDAN 2), from neutrino telescopes Baikal and AMANDA, and the most recent results from MINOS (LBL NuMI  $\nu_\mu$  beam and atmospheric  $\nu_s$ ) and MiniBooNE (SBL NuMI  $\nu_\mu$  beam).



## How to sum contributions into the $\nu N$ cross section?

It is conventional to estimate the inclusive CC and NC  $\nu N$  and  $\bar{\nu} N$  cross sections by the sum of contributions from exclusive channels and deep inelastic scattering (DIS):

$$\sigma_{\nu N}^{\text{tot}} = \sigma_{\nu N}^{(\text{Q})\text{ES}} \oplus \sigma_{\nu N}^{1\pi} \oplus \sigma_{\nu N}^{2\pi} \oplus \dots \oplus \sigma_{\nu N}^{1K} \oplus \dots \oplus \sigma_{\nu N}^{\text{DIS}}. \quad (1)$$

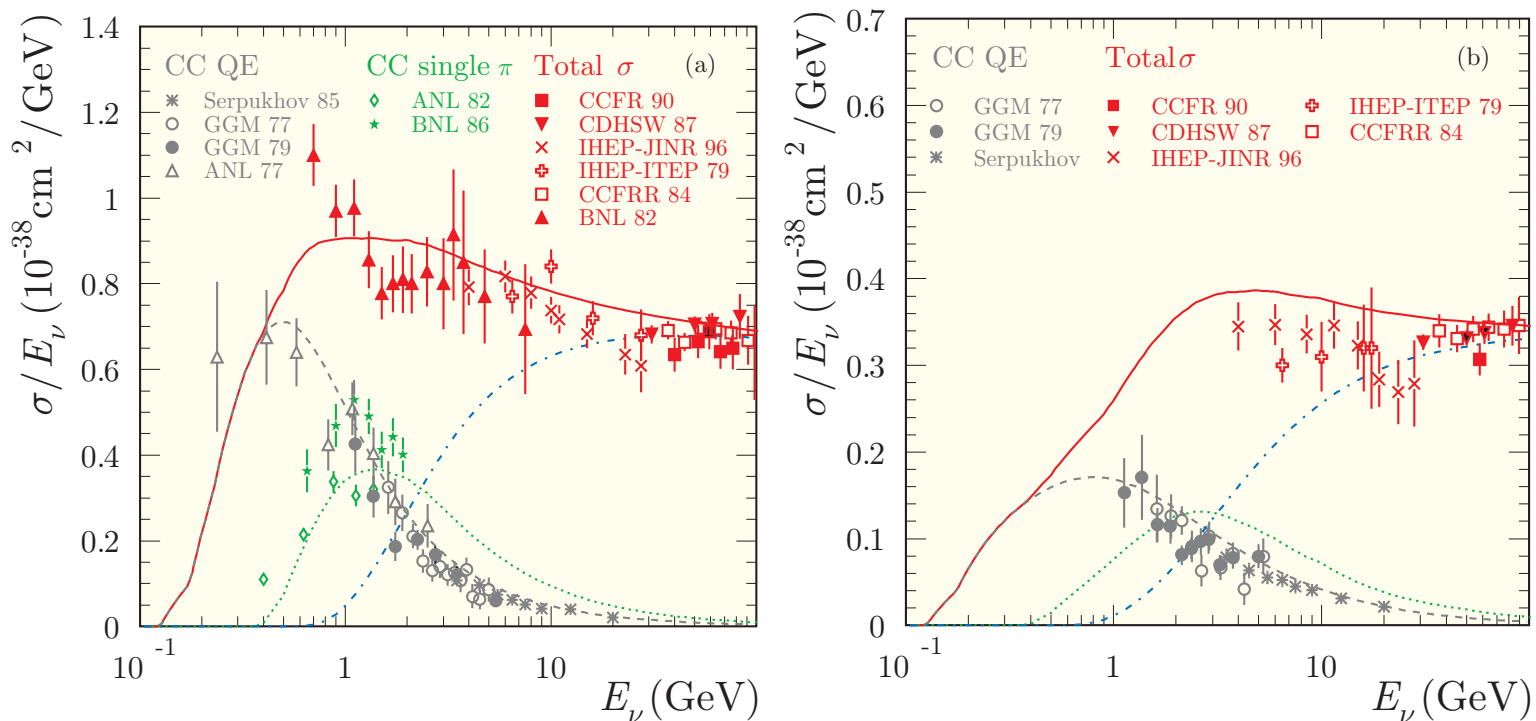
In the absence of a received model for multi-hadron exclusive neutrino production, the exclusive contributions in Eq. (1) are usually assumed to be saturated by elastic (NC case) or quasielastic (CC case) scattering (ES/QES) and single-pion production through baryon resonances (RES) and Eq. (1) simplifies to

$$\sigma_{\nu N}^{\text{tot}} = \sigma_{\nu N}^{(\text{Q})\text{ES}} \oplus \sigma_{\nu N}^{\text{RES}} \oplus \sigma_{\nu N}^{\text{DIS}} \quad (\text{“poor man” approximation}). \quad (2)$$

The exclusive and inclusive (DIS) contributions are of the **same order of magnitude** within the few-GeV energy region. Thus, to avoid double counting, the phase space of the RES and DIS contributions have to be scratched by the conditions

$$W < W_{\text{cut}}^{\text{RES}} \quad \text{and} \quad W > W_{\text{cut}}^{\text{DIS}},$$

respectively, where  $W$  is the invariant mass of the final hadron system in RES or DIS, and  $W_{\text{cut}}^{\text{RES}}$  and  $W_{\text{cut}}^{\text{DIS}}$  are some **unknown** parameters; the choice of these cutoffs is usually rather subjective.



The total CC cross sections (divided by  $E_\nu$ ) for  $\nu_\mu N$  and  $\bar{\nu}_\mu N$  including QES (dashed), single-meson productions (dot), and DIS (dash-dotted) adopted in the SK I experiment.<sup>a</sup>

$$M_A^{\text{QES}} = M_A^{\text{RES}} = 1.1 \text{ GeV}/c^2, \quad W_{\text{cut}}^{\text{RES}}(\text{RS}) = 2 \text{ GeV}, \quad W_{\text{cut}}^{\text{DIS}}(\text{GRV 94}) = 1.3 \text{ GeV};$$

the pion multiplicity  $n_\pi$  is restricted by the condition  $n_\pi \geq 2$  for  $1.3 < W < 2.0 \text{ GeV}$ .

<sup>a</sup>Y. Ashie *et al.* (Super-Kamiokande Collaboration), "A measurement of atmospheric neutrino oscillation parameters by Super-Kamiokande I," Phys. Rev. D **71** (2005) 112005 [arXiv:hep-ex/0501064].

The problem is aggravated by the uncertainties in the knowledge of the simplest exclusive contributions:

- The theoretical description of exclusive reactions for pion neutrino production through baryon resonances (RES) is vastly model-dependent.
- Even within a fixed model for RES, both RES and (Q)ES cross sections are very sensitive to the poorly known shape of the weak axial-vector form factors (phenomenologically described with by “axial masses”  $M_A^{\text{QES}}$  and  $M_A^{\text{RES}}$  whose experimental values spread within inadmissibly wide ranges.

---

In this study, we attempt to fine-tune (**within a single phenomenological approach**) the axial masses  $M_A^{\text{QES}}$ ,  $M_A^{\text{RES}}$  and the cutoffs  $W_{\text{cut}}^{\text{RES}}$ ,  $W_{\text{cut}}^{\text{DIS}}$  by a statistical analysis of all available experimental data on total and differential cross sections for

- quasielastic production of  $p$ ,  $n$ ,  $\Lambda^0$ ,  $\Sigma^-$ ,  $\Sigma^0$ ,
- baryon resonance and single-pion production,
- inclusive reactions,

as well as

- independently measured ratios of the cross sections for different channels.
- Average kinematic characteristics ( $\langle x \rangle$ ,  $\langle y \rangle$ ,  $\langle Q^2 \rangle$ , etc.).

All this for different nuclear targets.

---

Modest gains of this study is in demonstration of the uncertainties caused by variations of the poorly known input parameters and indetermination of the parton density functions (PDFs) within the single phenomenological approach.

---

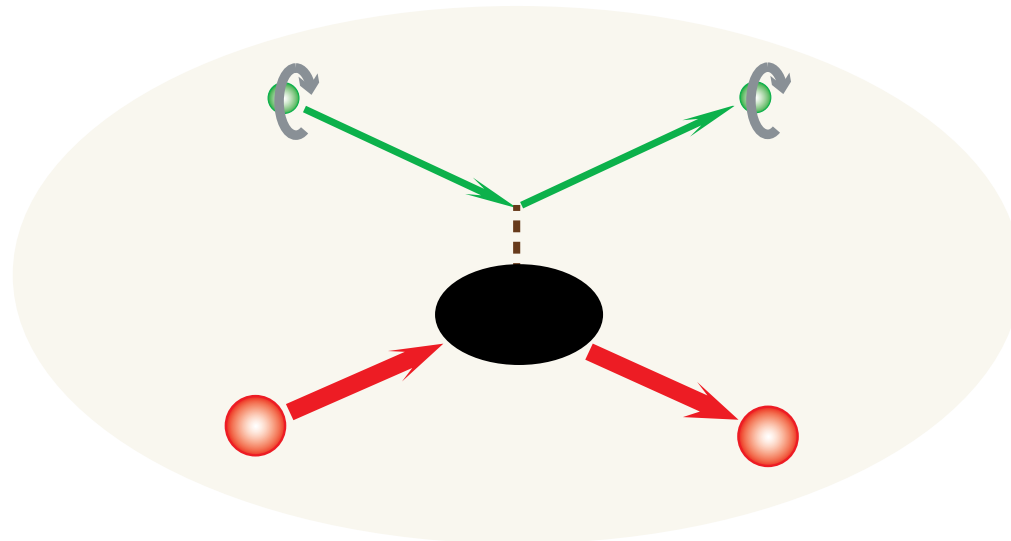
The problem under consideration is not 'fundamental' but its incorrect solution may lead to quite fundamental errors in the interpretation of the present and future neutrino experiments.

---

Currently, our likelihood analysis does not include several important subsamples of the world data and many theoretical omissions and simplifications.

So the results under discussion are yet **preliminary**.

# QUASIELASTIC SCATTERING



The most general formula for the QES cross section is<sup>a</sup>

$$\frac{d\sigma^{\text{QES}}}{dQ^2} = \frac{G_F^2 \cos^2 \theta_C M^2 \kappa^2}{2\pi E_\nu^2} \left[ A(q^2) + \left( \frac{s-u}{4M^2} \right) B(q^2) + \left( \frac{s-u}{4M^2} \right)^2 C(q^2) \right],$$

$$A = A_1 + 4A_2, \quad B = B_1 + 4B_2, \quad C = C_1 + 4C_2,$$

where indices “1” and “2” mark the FCC and SCC contribution, respectively, and

$$\begin{aligned} A_1 &= 2 \left[ (x' + r^2) (2x' + \kappa^2) - \kappa^4 \right] \text{Re} (F_V^* F_M) \\ &\quad \mp 4r \kappa^2 \text{Re} [F_A^* (F_V + F_M)] - 4\kappa^2 (x' + r^2 + \kappa^2) \text{Re} (F_A^* F_P) \\ &\quad + [(x' + \kappa^2) (x' - 1 + r^2 - \kappa^2) + r^2] |F_V|^2 \\ &\quad + [(x' + \kappa^2) (x' + 1 - r^2 - \kappa^2) + r^2] |F_A|^2 \\ &\quad - [x' (x' + r^2) (x' - 1 + \kappa^2) + \kappa^4] |F_M|^2 \\ &\quad + 4\kappa^2 (x' + \kappa^2) (x' + r^2) |F_P|^2, \\ B_1 &= \mp 4x' \text{Re} [F_A^* (F_V + F_M)] - 2r \kappa^2 \left[ |F_M|^2 + \text{Re} (F_V^* F_M + 2F_A^* F_P) \right], \\ C_1 &= |F_V|^2 + |F_A|^2 + x' |F_M|^2; \end{aligned}$$

---

<sup>a</sup>K. S. Kuzmin *et al.*, “Tau lepton polarization in quasielastic neutrino-nucleon scattering,” Nucl. Phys. B (Proc. Suppl.) **139** (2005) 154–157 [arXiv:hep-ph/0408107].

$$\begin{aligned}
A_2 &= -r(x' + r^2) [(x' + 1 + \varkappa^2) \operatorname{Re}(F_T^* F_A) + 2\varkappa^2 \operatorname{Re}(F_T^* F_P)] \\
&\quad - r\varkappa^2 [(x' + 1 + \varkappa^2) \operatorname{Re}(F_S^* F_V) + \varkappa^2 \operatorname{Re}(F_S^* F_M)] \\
&\quad - (x' + r^2) [(x' + \varkappa^2)(x' + 1 + r^2) + r^2] |F_T|^2 \\
&\quad + \varkappa^2 (x' + 1)(x' + \varkappa^2) |F_S|^2, \\
B_2 &= \varkappa^2 \operatorname{Re} \{ F_T^* [F_A - 2(x' + r^2) F_P] - F_S^* (F_V - x' F_M) \}, \\
C_2 &= r \operatorname{Re}(F_T^* F_A) + (x' + r^2) |F_T|^2.
\end{aligned}$$

In the above formulae,

$$\begin{aligned}
s &= (k + p)^2, \quad u = (k' - p)^2, \quad M = \frac{M_p + M_n}{2}, \quad \kappa = \frac{M_W^2}{M_W^2 + Q^2}; \\
x &= \frac{Q^2}{2(pq)}, \quad x' = \frac{Q^2}{4M^2}, \quad r = \frac{M_f - M_i}{M_f + M_i} = \frac{M_f - M_i}{2M}, \quad \text{and} \quad \varkappa = \frac{m_\ell}{2M}.
\end{aligned}$$

In the standard model limit ( $F_S = F_T = 0$ ) our formula reduces to that of Strumia and Vissani<sup>a</sup> derived for the inverse  $\beta$  decay taking account the proton-neutron mass difference. Below we apply just this standard model result.

---

<sup>a</sup>A. Strumia and F. Vissani, "Precise quasielastic neutrino/nucleon cross-section," Phys. Lett. B **564** (2003) 42–54 [arXiv:astro-ph/0302055].

## Vector form factors

The Dirac and Pauli vector form factors  $F_{V,M}$  are related to the Sachs electric and magnetic form factors  $G_{E,M}$ :

$$F_V = \frac{G_E + x' G_M}{1 + x'}, \quad F_M = \frac{G_M - G_E}{1 + x'}, \quad (x' = \frac{Q^2}{4M^2}).$$

Isotopic symmetry provides simple relation between  $G_{E,M}$  and elastic electric and magnetic form factors of proton and neutron  $G_E^{p,n}$  and  $G_M^{p,n}$ :

$$G_M = G_M^p - G_M^n, \quad G_E = G_E^p - G_E^n.$$

At low  $Q^2$ , a reasonable description is given by the *dipole approximation*:

$$G_E^p \approx G_D, \quad G_M^p \approx \mu_p G_D, \quad G_E^n \approx 0, \quad G_M^n \approx \mu_n G_D,$$
$$G_D = (1 + Q^2/M_V^2)^{-2}, \quad M_V = 0.84 \text{ GeV}/c^2,$$

where  $\mu_p$  ( $\mu_n$ ) is the anomalous magnetic moment of the proton (neutron).

*Analyses of almost all earlier neutrino experiments were based on this approximation.*

In this study, we utilize two more sophisticated models for  $G_E^{p,n}$  and  $G_M^{p,n}$ :  
BBBA(07) and GKex(05).

## BBBA(07) model<sup>a</sup>

The BBBA(07) model is an accurate Kelly type parametrization of the current experimental data on the form factors  $G_E^p$ ,  $G_M^p$ ,  $G_E^n$ ,  $G_M^n$ , and ratio  $G_E^p/G_M^p$ , which uses the Nachtmann scaling variable  $\xi_{p,n} = 2 \left(1 + \sqrt{1 + 4M_{p,n}^2/Q^2}\right)^{-1}$ , to relate elastic and inelastic form factors, and imposes quark-hadron duality (QHD) asymptotic constraints at high momentum transfers where the quark structure dominates. QHD implies that the squared ratio of  $G_M^n$  and  $G_M^p$  should be the same as the ratio of the corresponding inelastic structure functions  $F_2^n$  and  $F_2^p$  in the limit  $\xi_{p,n} = 1$ :

$$\left(\frac{G_M^n}{G_M^p}\right)^2 = \frac{F_2^n}{F_2^p} = \frac{1 + 4(d/u)}{4 + (d/u)}, \quad Q^2 \rightarrow \infty.$$

Here  $d$  and  $u$  are the partonic density functions. The authors fit the data under the two assumptions:  $d/u = 0$  and  $d/u = 0.2$ .

One more duality-motivated constraint is the asymptotic equality

$$(G_E^n/G_M^n)^2 = (G_E^p/G_M^p)^2, \quad Q^2 \rightarrow \infty,$$

applied for the highest  $Q^2$  data points for  $G_E^n$  included into the BBBA(07) fit.

---

<sup>a</sup>A. Bodek, S. Avvakumov, R. Bradford, and H. Budd, "Duality constrained parameterization of vector and axial nucleon form factors," Eur. Phys. J. C **53** (2008) 349–354; arXiv:0708.1946 [hep-ex] (see also arXiv:0708.1827 [hep-ex]).

## GKex(05) model<sup>a</sup>

The GKex(05) model is in fact a modification of the QCD inspired vector dominance model (VDM) by [Gari and Krüempelmann \(GK\)](#)<sup>b</sup> extended and fine-tuned by Lomon<sup>c</sup> in order to match the current and consistent earlier experimental data. The data set used by Lomon includes the polarization transfer measurements, which are directly related to the ratios of electric to magnetic form factors, and differential cross section measurements of the magnetic form factors. The electric form factors derived from the Rosenbluth separation of the differential cross section are only used for the lower range of  $Q^2$  where the magnetic contributions are less dominant.

Among several versions of the parametrization considered by Lomon, we chose the latest one “GKex(05)” described in Ref. arXiv:nucl-th/0609020. This version incorporates the data that has become available since the previous publication by Lomon.

The fitted parameters agree with known constraint and the model is consistent with VDM at low  $Q^2$ , while approaching perturbative QCD behavior at high  $Q^2$ .

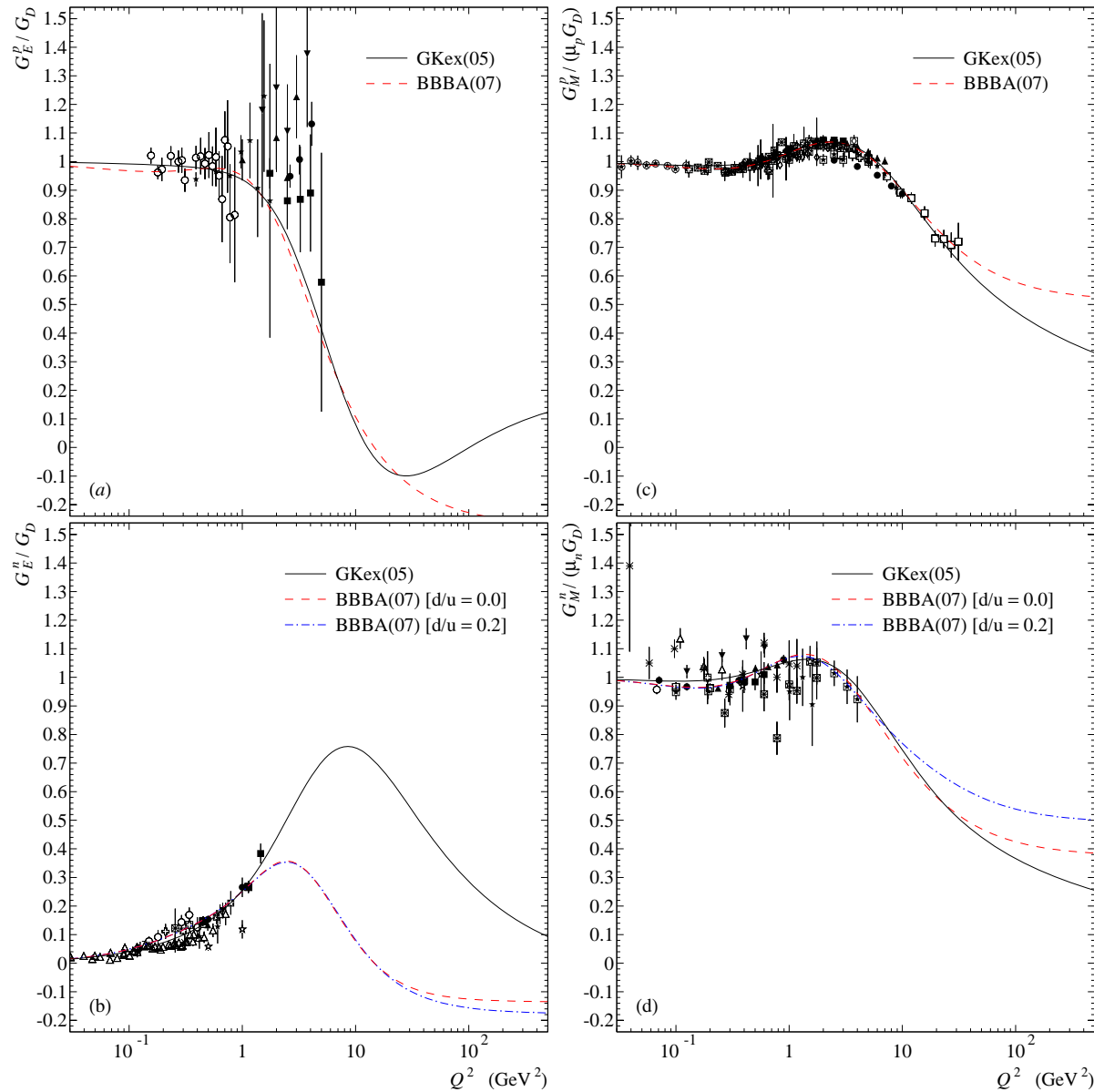
[The quark-hadron duality constraint is not imposed.](#)

---

<sup>a</sup>E. L. Lomon, “Effect of revised  $R_n$  measurements on extended Gari-Krüempelmann model fits to nucleon electromagnetic form factors,” arXiv:nucl-th/0609020.

<sup>b</sup>M. F. Gari and W. Krüempelmann, “The electric neutron form-factor and the strange quark content of the nucleon,” Phys. Lett. B **274** (1992) 159; *ibid.* **282** (1992) 483 (E).

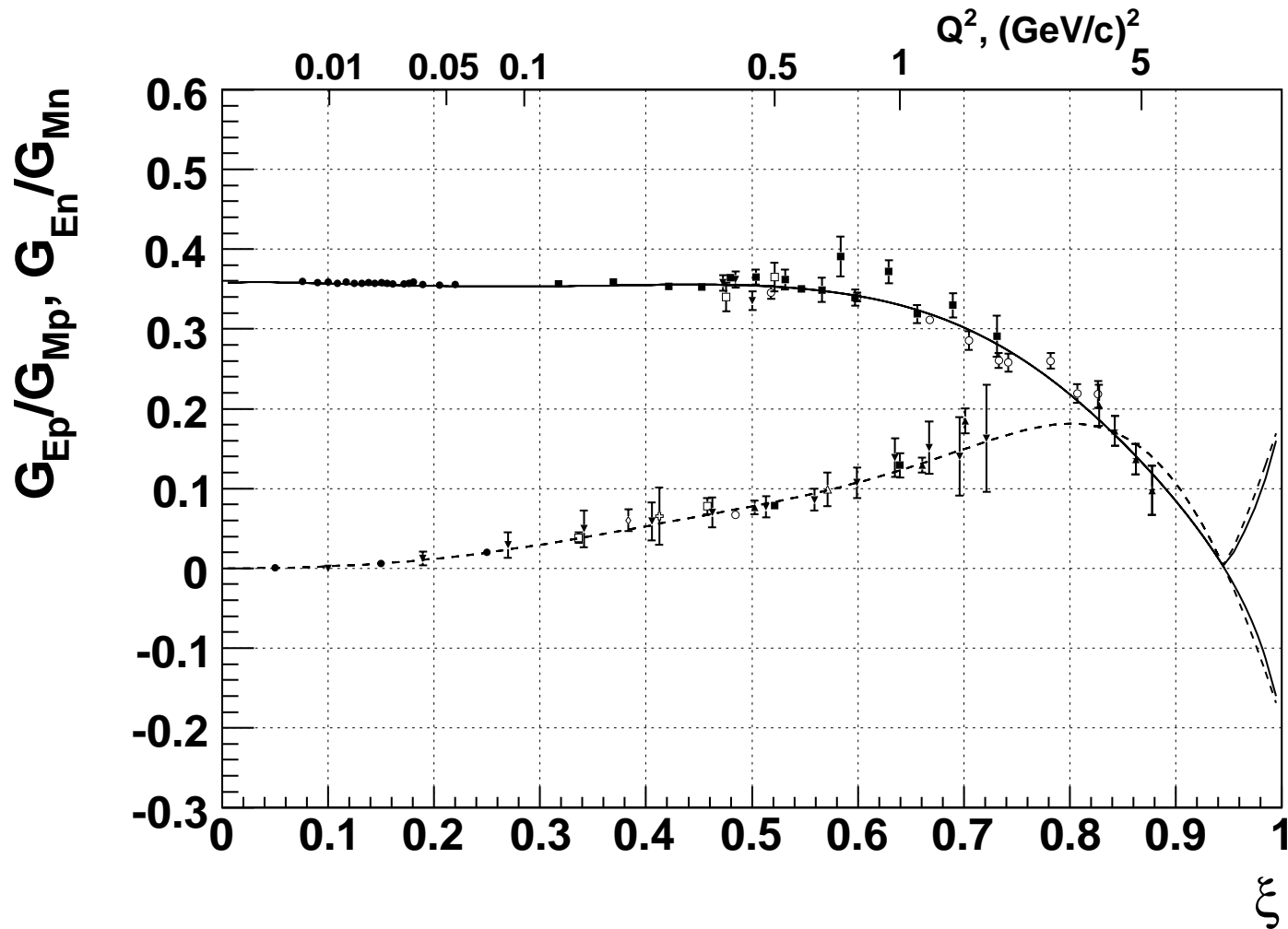
<sup>c</sup>E. L. Lomon, “Extended Gari-Krüempelmann model fits to nucleon electromagnetic form factors,” Phys. Rev. C **64** (2001) 035204 [arXiv:nucl-th/0104039]; E. L. Lomon, “Effect of recent  $R_p$  and  $R_n$  measurements on extended Gari-Krüempelmann model fits to nucleon electromagnetic form factors,” Phys. Rev. C **66** (2002) 045501 [arXiv:nucl-th/0203081].



Comparison of the GKex(05) and BBBA(07) models for the vector form factors of  $p$  and  $n$  with the data extracted mainly from electron scattering experiments using either the Rosenbluth separation or polarization transfer techniques.

The data compilation is taken from many sources.

The most serious disagreement between the two models is in the neutron electric form factor at  $Q^2 \gtrsim 2 \text{ GeV}^2$ .



The constraint used in the  $\text{BBBA}(07)_{d/u=0}$  fitting electric neutron form factor  $G_E^n$  stipulates that  $(G_E^n/G_M^n)^2 = (G_E^p/G_M^p)^2$  at high  $\xi_{p,n}$ . The solid line is  $G_E^p/|G_M^p|$  and  $|G_E^p|/|G_M^p|$ , and the short-dashed line is  $G_E^n/|G_M^n|$  and  $|G_E^n|/|G_M^n|$ . [From [arXiv:0708.1946 \[hep-ex\]](https://arxiv.org/abs/0708.1946).]

## Axial-vector and induced pseudoscalar form factors

For the axial and pseudoscalar form factors we use the conventional parametrizations

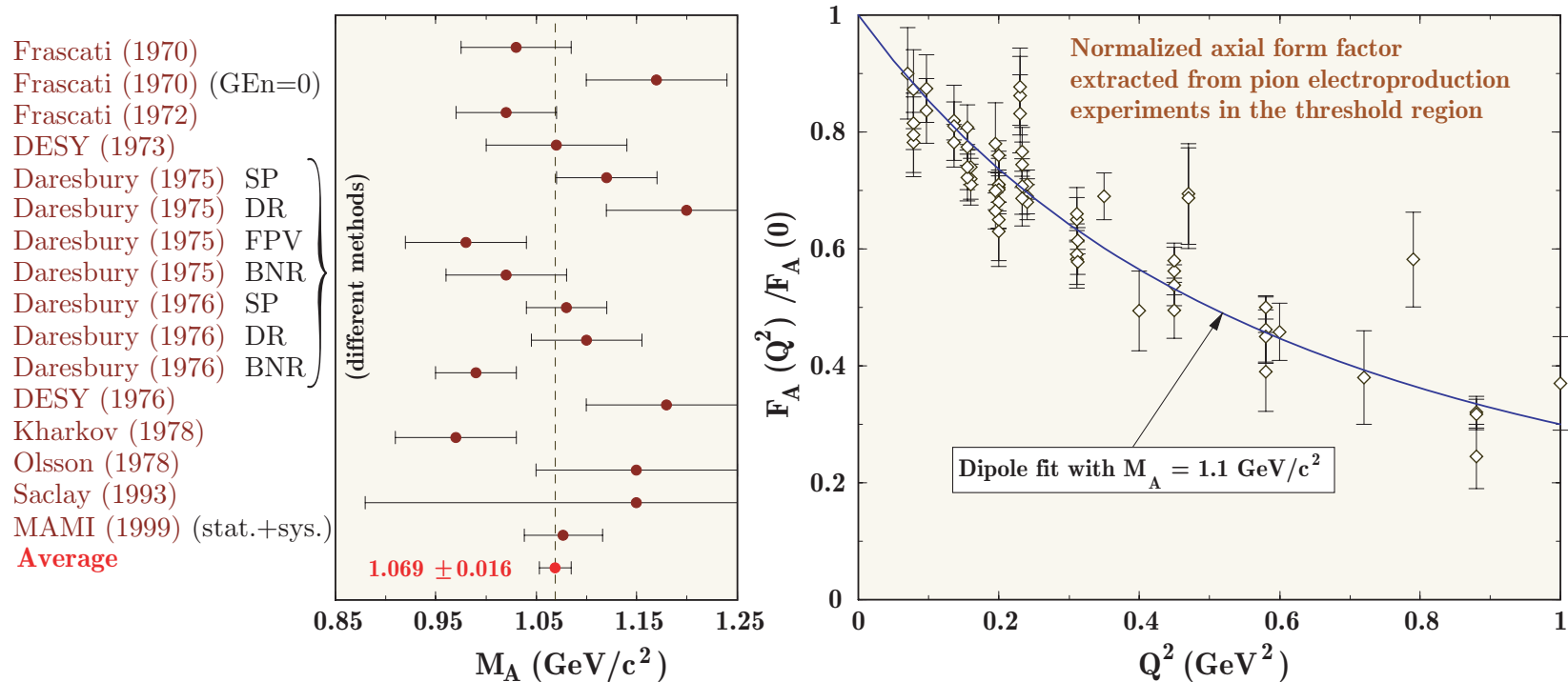
$$F_A(Q^2) = F_A(0) \left( 1 + \frac{Q^2}{M_A^2} \right)^{-2}, \quad (3)$$

$$F_P(Q^2) = \frac{2M^2}{m_\pi^2 + Q^2} F_A(Q^2), \quad (4)$$

where  $F_A(0) = g_A$  is the axial coupling,  $m_\pi$  is the charged pion mass, and  $M_A$  is the axial-vector mass treated as a free parameter. In fact, Eq. (4) is a conjecture inspired by the hypothesis of partial conservation of the axial current (PCAC), expectation that the form factor  $F_P$  is dominated by the pion pole near  $Q^2 = 0$ , and the “technical” condition

$$m_\pi^2 \left| \frac{1}{F_A(0)} \frac{dF_A(Q^2)}{dQ^2} \right|_{Q^2=0} = \frac{2m_\pi^2}{M_A^2} \ll 1,$$

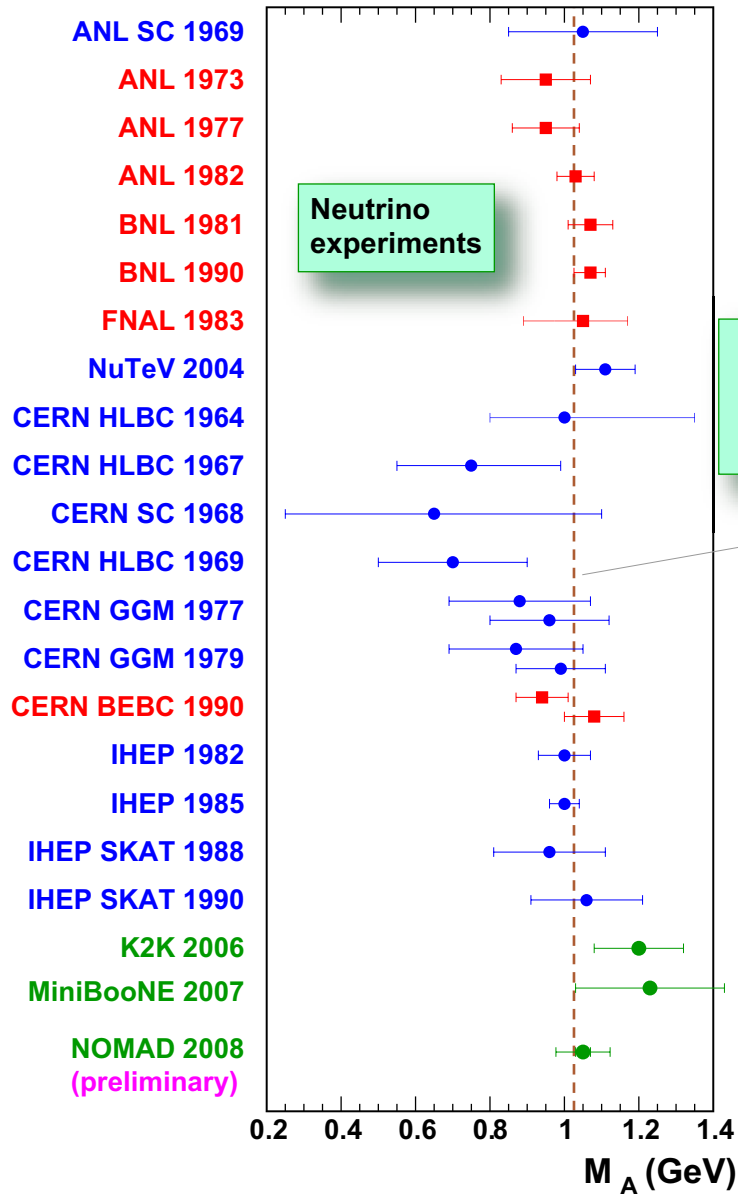
which is obviously fulfilled for the experimental lower limit of  $M_A$ . Considering that the pseudoscalar contribution enters into the cross sections multiplied by  $(m_e/M)^2$ , the uncertainty caused by this approximation may only be significant for  $\nu_\tau/\bar{\nu}_\tau$  induced reactions and it is not very important for reactions induced by  $\nu_{e,\mu}/\bar{\nu}_{e,\mu}$ .



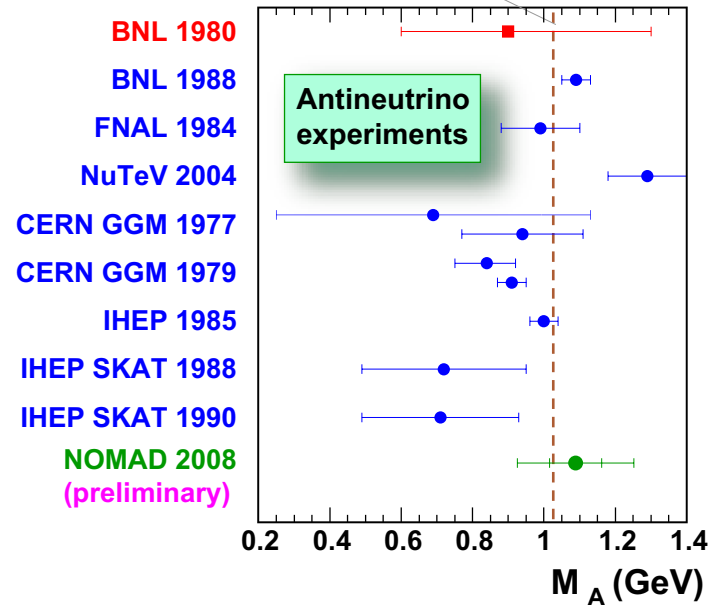
Axial mass (left panel) and the normalized axial form factor (right panel) extracted from pion electroproduction experiments. Both compilations are borrowed from review by V. Bernard *et al.*<sup>a</sup> Only statistical errors are included in the left figure, except for the MAMI (1999) experiment. Note that the results for  $M_A$  and  $F_A$  extractions are very model dependent.

It is seen that the pion electroproduction experiments permit very wide spread of  $M_A$ :

<sup>a</sup>V. Bernard, L. Elouadrhiri and Ulf-G. Meißner, "Axial structure of the nucleon," J. Phys. G **28** (2002) R1–R35 [arXiv:hep-ph/0107088].



Old world average value,  $1.026 \pm 0.021$  GeV according to V. Bernard et al., J. Phys. G 28 (2002) R1-R35 [arXiv:hep-ph/0107088]



## BBBA(07) Re-extraction<sup>a</sup>

Experiment	QE ev.	$Q^2$ range (GeV/c) <sup>2</sup>	$\langle E_\nu \rangle$ (GeV)	Vector FF used	$-g_A, M_V^2$ used	$M_A$ (publ.)	$\Delta M_A$ FF, RC	$M_A$ (updated)
<b>Neutrino-deuterium experiments</b>								
ANL 73	166	0.05–1.6	0.7	B $G_e^n = 0$	1.23, 0.84 <sup>2</sup>	0.95 ± 0.12	-0.030, 0.002	0.972 ± 0.05
ANL 77	500	0.05–1.6	0.7	O $G_e^n = 0$	1.23, 0.84 <sup>2</sup>	0.95 ± 0.09	-0.026, 0.002	
ANL 82	1737	0.05–2.5	0.7	O $G_e^n = 0$	1.23, 0.84 <sup>2</sup>	1.00 ± 0.05	-0.030, 0.002	
BNL 81	1138	0.06–3.0	1.6	O $G_e^n = 0$	1.23, 0.84 <sup>2</sup>	1.07 ± 0.06	-0.028, 0.002	1.044 ± 0.06
FNAL 83	362	0.11–3.0	20	O $G_e^n = 0$	1.23, 0.84 <sup>2</sup>	1.05 <sup>+0.12</sup> <sub>-0.16</sub>	-0.025, 0.001	1.026 <sup>+0.12</sup> <sub>-0.16</sub>
BNL 90	2544	0.10–3.0	1.6	O $G_e^n = 0$	1.254, 0.84 <sup>2</sup>	1.070 <sup>+0.040</sup> <sub>-0.045</sub>	-0.036, 0.002	1.036 <sup>+0.040</sup> <sub>-0.045</sub>
BEBC 90	552	0.1–3.75	20	D $G_e^n = 0$	1.255, 0.84 <sup>2</sup>	1.080 ± 0.08	-0.080, 0.002	1.002 ± 0.08
<b>Av. <math>\nu_\mu</math>-d</b>	5780	above		BBBA(07)	1.267, 0.71	1.051 ± 0.026	$\theta_\mu, E_\mu, \theta, P_p$	<b>1.016 ± 0.026</b>
<b>Pion electroproduction</b>								<b>1.014 ± 0.016</b>
<b>Antineutrino-hydrogen experiment</b>								
BNL 81	13	0–1.0	1.1	D $G_e^n = 0$	1.23, 0.84 <sup>2</sup>	0.9 ± 0.35	-0.070, 0.01	0.831 ± 0.35
BNL 81	13	0–1.0	1.1	BBBA(07)	1.267, 0.71	$\sigma_{QE}$	$\theta_\mu, E_\mu$	1.04 ± 0.40
<b>Average all</b>								<b>1.014 ± 0.014</b>

$M_A$  (GeV/c<sup>2</sup>) values published by  $\nu_\mu$ -d experiments and updated corrections  $\Delta M_A$  when re-extracted with updated BBBA(07) form factors, and  $g_A = -1.267$ . Also shown are  $M_A$  from pion electroproduction data and updated  $M_A$  from BNL  $\bar{\nu}_\mu$ -H data.

<sup>a</sup>A. Bodek, S. Avvakumov, R. Bradford, and H. Budd, “Duality constrained parameterization of vector and axial nucleon form factors,” Eur. Phys. J. C **53** (2008) 349–354; arXiv:0708.1946 [hep-ex] (see also arXiv:0708.1827 [hep-ex]).

## Nuclear effects

Since the main part of the experimental data on the QES cross sections for nuclear targets was not corrected for nuclear effects, we must take these into account in our calculations. In the present study, we use the [Relativistic Fermi gas model \(RFG\)](#) model by Smith and Moniz<sup>a</sup> incorporated as a standard tool into essentially all neutrino event generators employed in accelerator and astroparticle neutrino experiments.

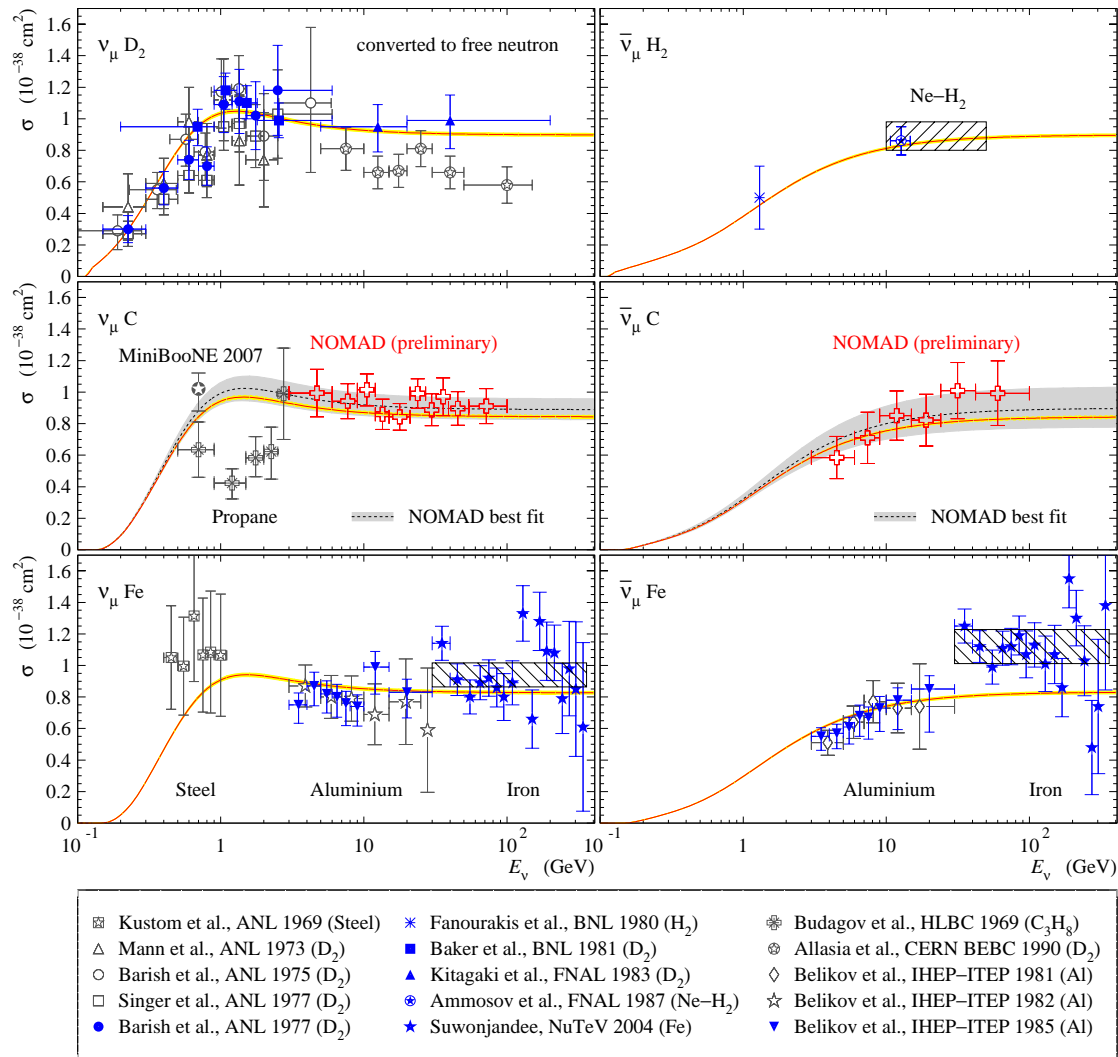
In the RFG model, the nuclear structure functions  $T_i$  which take into account the [Fermi motion](#) and [Pauli blocking](#) effects, and [binding energy](#) for nuclear targets, are the linear combination of the standard free-nucleon SFs  $W_i$  with coefficients which involve the Fermi distribution functions.

---

<sup>a</sup>R. A. Smith and E. J. Moniz, "Neutrino reactions on nuclear targets," Nucl. Phys. B **43** (1972) 605–622; erratum – *ibid.* **101** (1975).

Values of Fermi momenta and binding energies (in MeV) for selected nuclei.

Nucleus	$p_F^p$	$\epsilon_p$	$p_F^n$	$\epsilon_n$
Li <sub>7</sub> <sup>3</sup>	169	15.1	169	15.1
C <sub>12</sub> <sup>6</sup>	221	25.7	221	25.6
N <sub>14</sub> <sup>7</sup>	223	26.2	223	26.1
O <sub>16</sub> <sup>8</sup>	225	26.6	225	26.6
F <sub>19</sub> <sup>9</sup>	233	28.4	233	28.3
Ne <sub>20</sub> <sup>10</sup>	230	27.8	230	27.8
Mg <sub>24</sub> <sup>12</sup>	235	29.0	235	28.9
Al <sub>27</sub> <sup>13</sup>	237	29.5	237	29.4
Si <sub>28</sub> <sup>14</sup>	239	30.0	239	29.9
Cl <sub>36</sub> <sup>17</sup>	240	30.2	244	31.2
Ar <sub>40</sub> <sup>18</sup>	242	30.7	259	35.0
Ca <sub>40</sub> <sup>20</sup>	251	33.0	251	32.9
Fe <sub>56</sub> <sup>26</sup>	251	33.0	263	36.1
Ni <sub>59</sub> <sup>28</sup>	257	34.6	263	36.1
Cu <sub>64</sub> <sup>29</sup>	257	34.6	263	36.1
Br <sub>80</sub> <sup>35</sup>	249	32.5	270	38.1
Sn <sub>119</sub> <sup>50</sup>	245	31.5	274	39.1
Pb <sub>207</sub> <sup>82</sup>	245	31.5	283	41.7



Total QES cross sections measured in experiments with deuterium, hydrogen, carbon/propane, aluminium, and iron/steel targets.

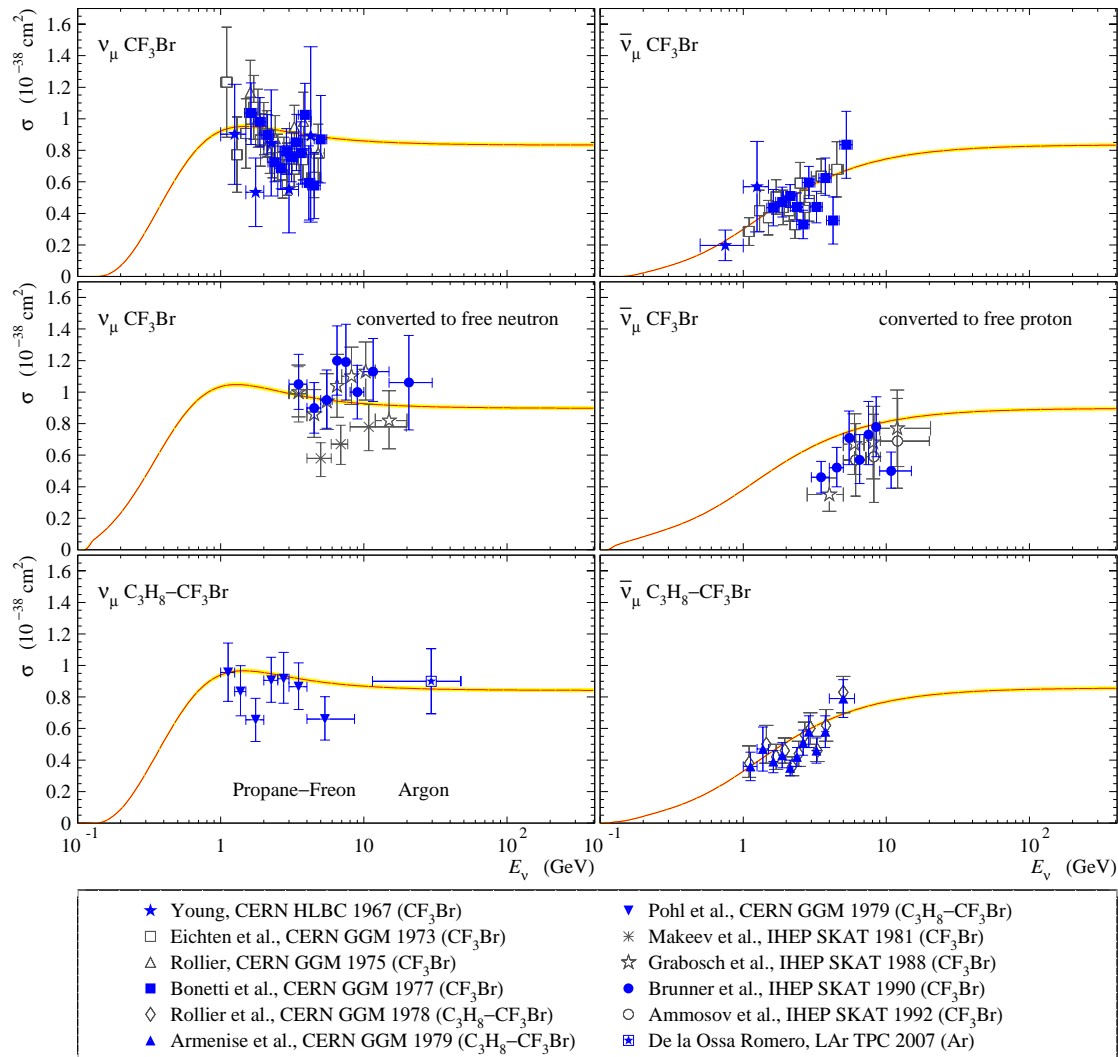
The error bars show the total errors which include the flux normalization uncertainties.

The solid curves and narrow shaded bands are calculated with the BBBA(07) model for the vector form factors, with

$$M_A = 0.999 \pm 0.011 \text{ GeV}/c^2,$$

the value obtained from the global fit to a subset of the full data set of total and differential cross sections (233 data points).

The MiniBooNE 2007 point recalculated from the reported value of  $M_A = 1.23 \pm 0.20 \text{ GeV}/c^2$  is also shown. The dashed curves with bands are the cross sections obtained by fitting the preliminary NOMAD 2008  $\nu_\mu$  and  $\bar{\nu}_\mu$  data separately (Lyubushkin's report in this workshop).



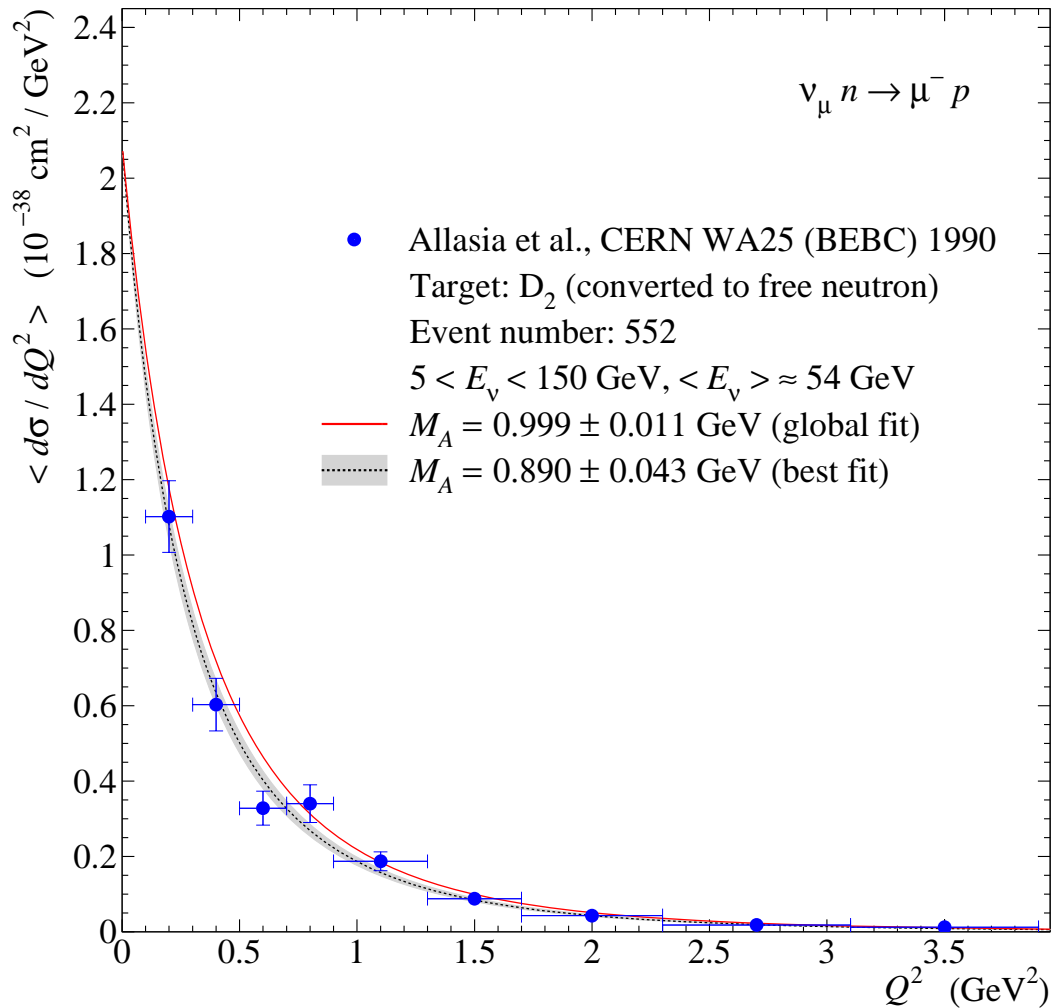
The error bars show the total errors which include the uncertainties due to normalization and nuclear Monte Carlo. The SKAT data are converted from freon to a free  $n/p$  target by the authors of the experiments.

Total QES cross sections measured in the freon and propane-freon filled bubble chamber experiments. The point recently obtained in experiment with the Liquid Argon Time Projection Chamber (LArTPC 2007) is also shown.

The solid curves and narrow shaded bands are calculated with the BBBA(07) model for the vector form factors, with

$$M_A = 0.999 \pm 0.011 \text{ GeV}/c^2,$$

the value obtained from the global fit to a subset of the full data set of total and differential cross sections (233 data points).

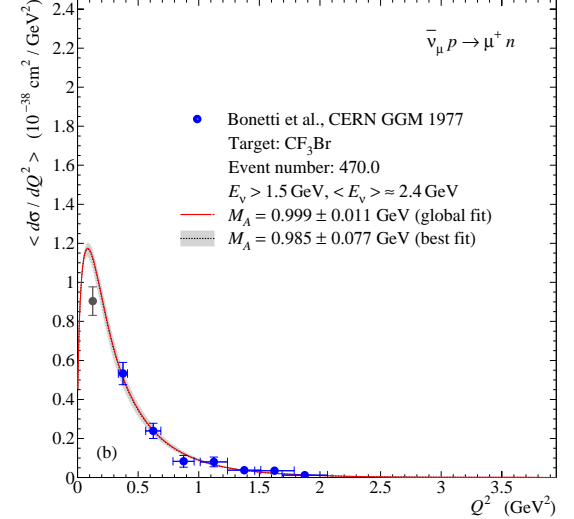
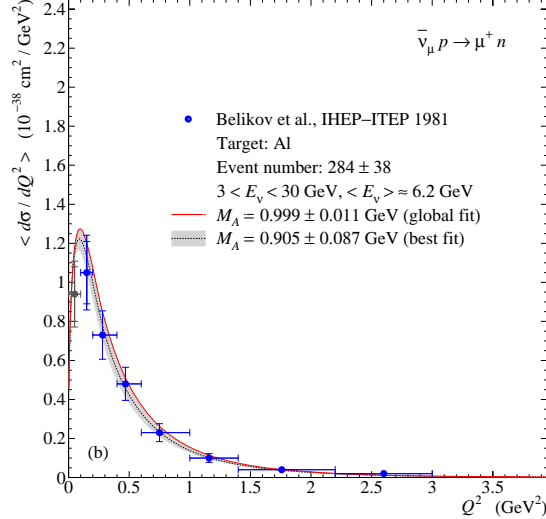
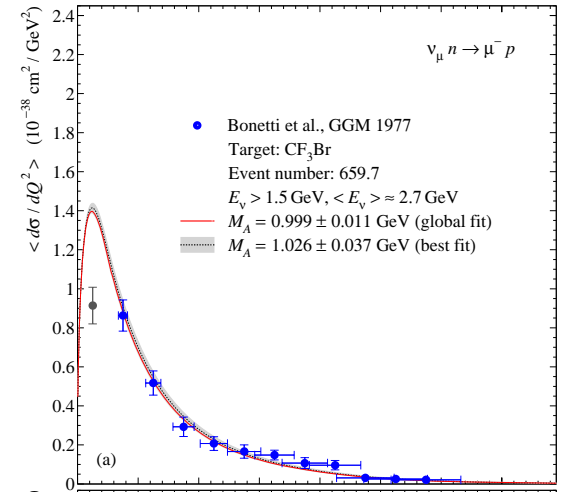
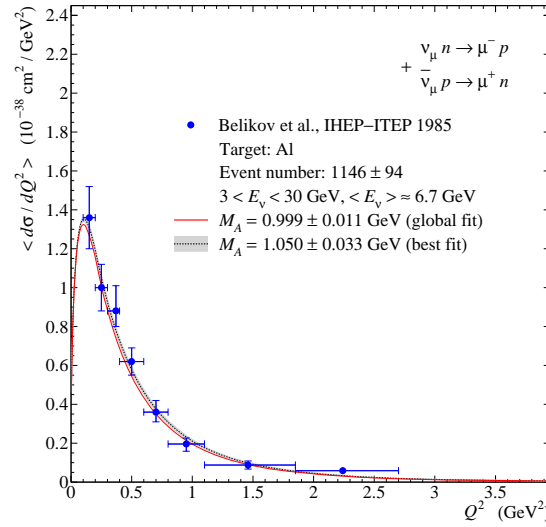
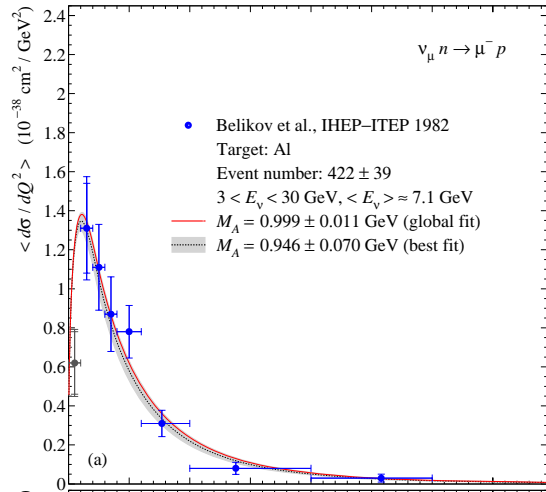


Flux weighted differential cross section for  $\nu_\mu n \rightarrow \mu^- p$  measured in the WA25 experiment with the CERN bubble chamber BEBC filled with deuterium and exposed to high-energy  $\nu_\mu$  beam at the CERN-SPS.

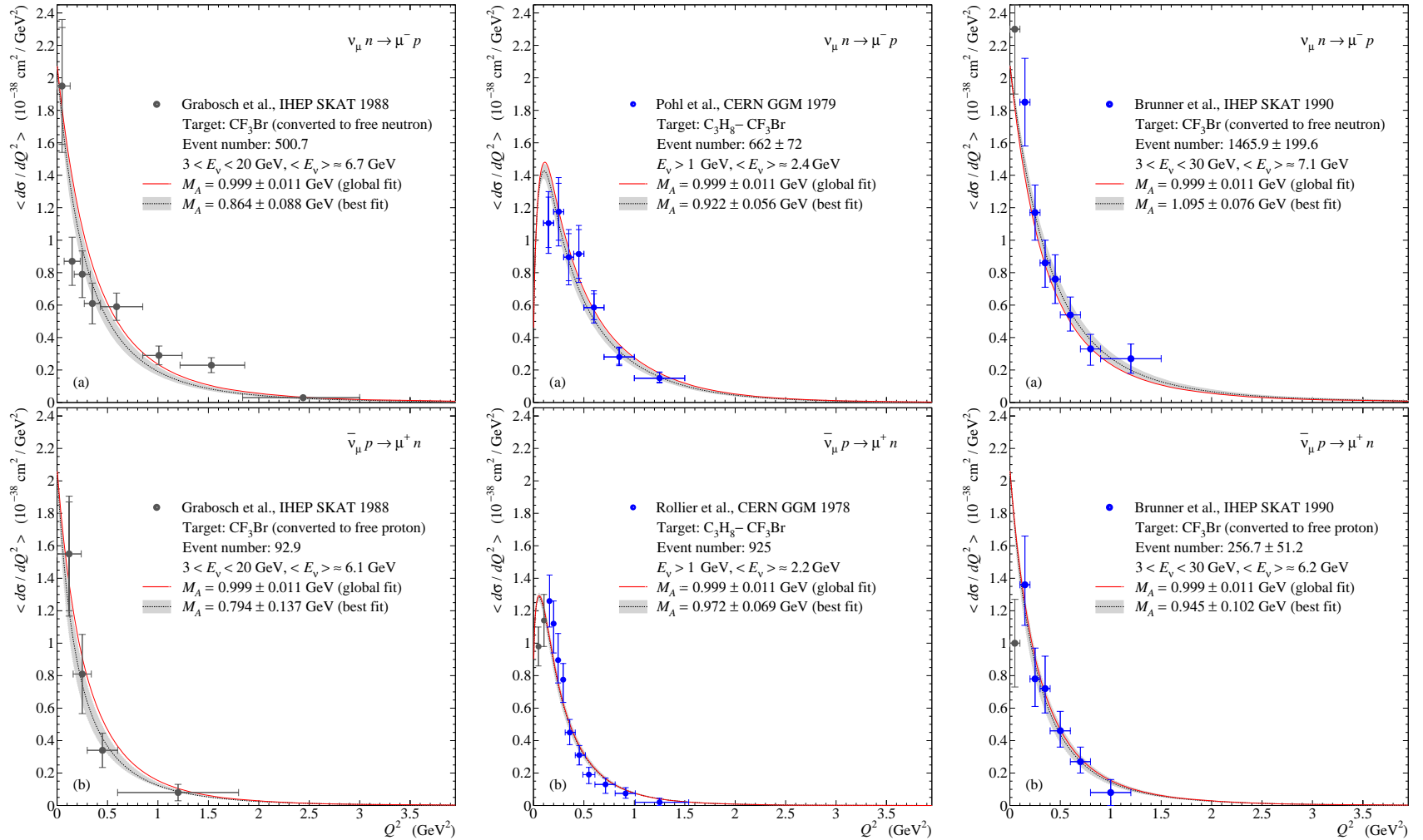
The data were converted to a free neutron target by the authors of the experiment.

The curves are the calculated cross sections averaged over the experimental  $\nu_\mu$  energy spectrum. The energy range and estimated mean energy are given in the legend.

The dashed curves are for the best fit to the WA25 data, while the solid curves correspond to the global fit through all QES data. The shaded bands show  $1\sigma$  deviation from the best-fitted value of  $M_A$  shown in the legend.



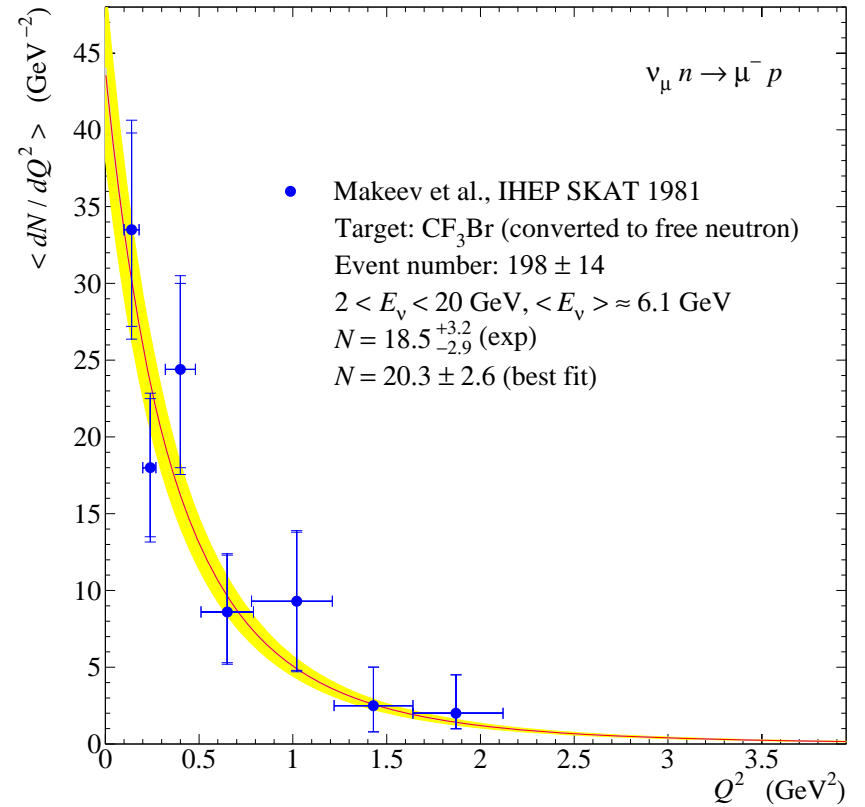
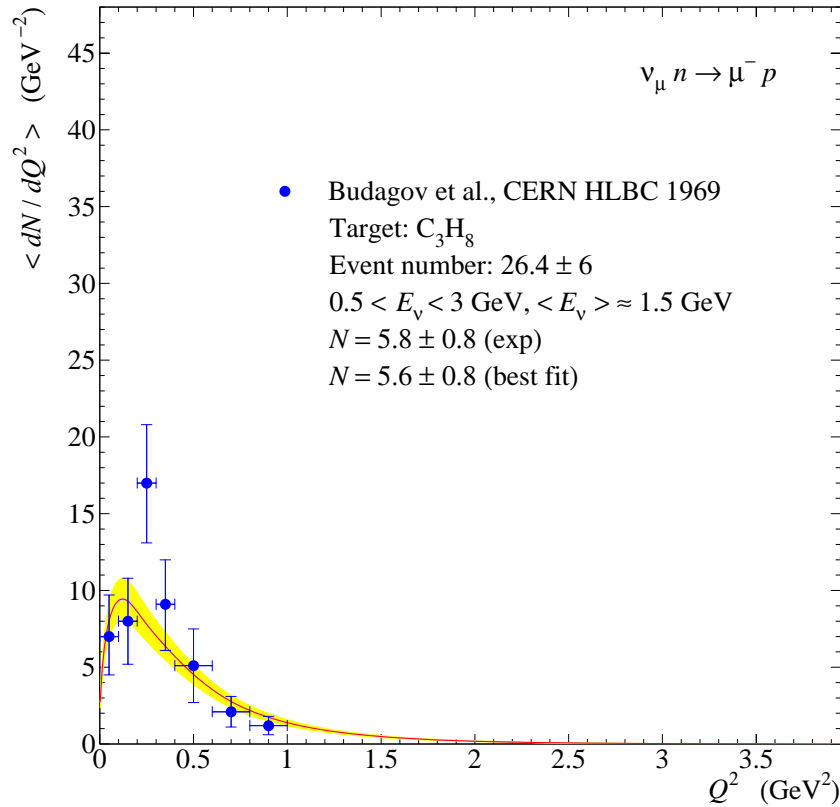
Flux weighted differential cross sections for  $\nu_\mu n \rightarrow \mu^- p$  and  $\bar{\nu}_\mu p \rightarrow \mu^+ n$  measured in the IHEP-ITEP experiments with a spark chamber detector with aluminium filters and exposed to the U70 broad-band  $\nu_\mu/\bar{\nu}_\mu$  beams of the Serpukhov PS, and the experiment with the heavy-liquid bubble chamber Gargamelle filled with heavy freon and exposed to the CERN-PS  $\nu_\mu/\bar{\nu}_\mu$  beams.



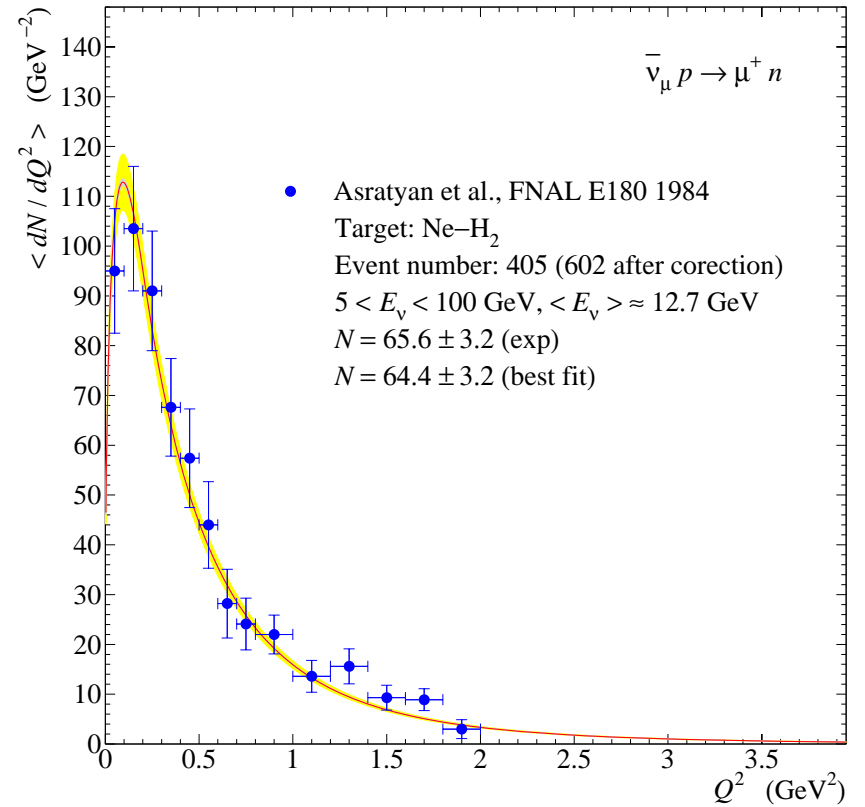
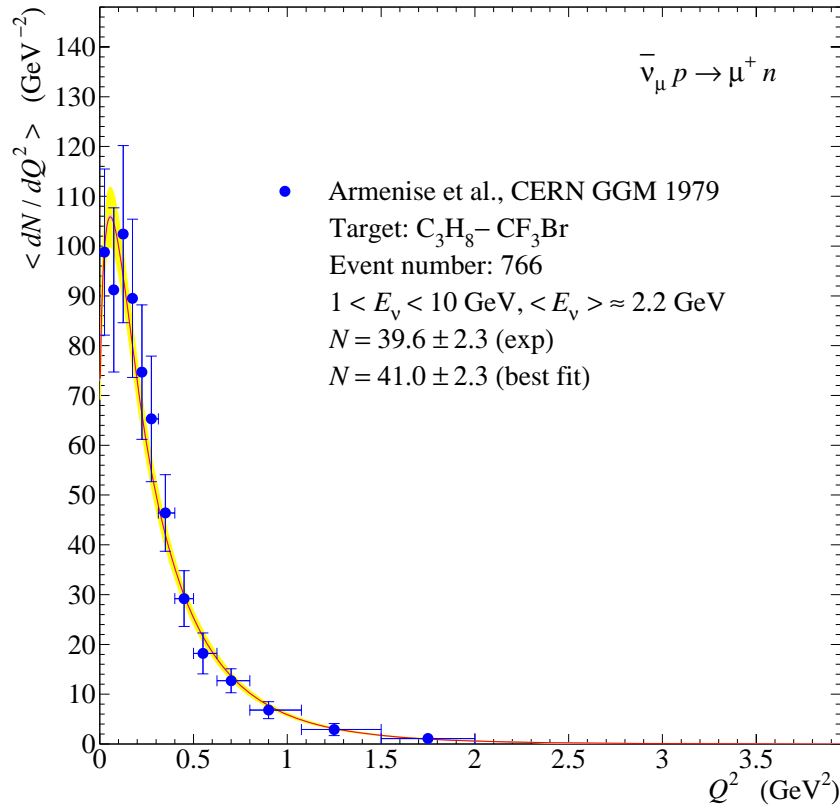
Flux weighted differential cross sections for  $\nu_\mu n \rightarrow \mu^- p$  and  $\bar{\nu}_\mu p \rightarrow \mu^+ n$  measured with the freon filled bubble chamber SKAT exposed to the U70 broad-band  $\nu_\mu/\bar{\nu}_\mu$  beams of the Serpukhov PS and with the bubble chamber Gargamelle filled with light propane–freon mixture and exposed to the CERN-PS  $\nu_\mu/\bar{\nu}_\mu$  beams.

Values of  $M_A$  (given in GeV), extracted by fitting the  $\nu_\mu$ ,  $\bar{\nu}_\mu$ , and  $\nu_\mu + \bar{\nu}_\mu$  data on total and differential QES cross sections, using the BBBA(07) and GKex(05) models for the vector form factors of the nucleon. The  $\chi^2/\text{NDF}$  values for each fit are shown in parentheses.

BBBA(07)			GKex(05)		
$M_A(\nu)$	$M_A(\bar{\nu})$	$M_A(\nu + \bar{\nu})$	$M_A(\nu)$	$M_A(\bar{\nu})$	$M_A(\nu + \bar{\nu})$
<b>Fit to the total cross sections</b>					
$0.994 \pm 0.017$ (83/82)	$1.047 \pm 0.025$ (134/62)	$1.011 \pm 0.014$ (220/145)	$0.986 \pm 0.017$ (83/82)	$1.035 \pm 0.025$ (137/62)	$1.001 \pm 0.014$ (222/145)
<b>Fit to the differential cross sections</b>					
$0.979 \pm 0.020$ (45/48)	$0.991 \pm 0.029$ (26/37)	$0.983 \pm 0.017$ (71/86)	$0.976 \pm 0.020$ (45/48)	$0.982 \pm 0.030$ (25/37)	$0.978 \pm 0.017$ (70/86)
<b>Fit to the total and differential cross sections</b>					
$0.988 \pm 0.013$ (128/131)	$1.023 \pm 0.018$ (163/100)	$0.999 \pm 0.011$ (293/232)	$0.981 \pm 0.013$ (128/131)	$1.012 \pm 0.019$ (163/100)	$0.991 \pm 0.011$ (293/232)



Flux weighted  $Q^2$  distributions for  $\nu_\mu n \rightarrow \mu^- p$  measured with the CERN heavy-liquid bubble chamber (HLBC) filled with propane and exposed to the CERN PS  $\nu_\mu$  beam and with the freon filled bubble chamber SKAT exposed to the U70 broad-band  $\nu_\mu$  beam of the Serpukhov PS. The data from SKAT were converted to a free nucleon target by the authors of the experiment. The curves are the distributions calculated with  $M_A$  obtained from the global fit, averaged over the experimental  $\nu_\mu$  energy spectra. The shaded bands shows  $1\sigma$  variation from the average due to uncertainties in  $M_A$  and normalization factor  $N$ .



Flux weighted  $Q^2$  distributions for  $\bar{\nu}_\mu p \rightarrow \mu^+ n$  measured with the bubble chamber Gargamelle filled with light propane–freon mixture (87 mole per cent of propane) and exposed to the CERN-PS  $\bar{\nu}_\mu$  beam, and in the FNAL E180 experiment with a 15' bubble chamber filled with heavy neon–hydrogen mixture (64% of neon atoms) and exposed to the FNAL wide-band  $\bar{\nu}_\mu$  beam. The curves are the distributions calculated with  $M_A$  obtained from the global fit, averaged over the experimental  $\bar{\nu}_\mu$  energy spectra. The shaded bands shows  $1\sigma$  variation from the average due to uncertainties in  $M_A$  and normalization factor  $N$ .

## Conclusions

Our statistical analysis of **full** set of the QES data (with  $\Delta Y = 0$ ) yields:

$$M_A^{\text{QES, BBBA(07)}} = 0.999 \pm 0.011 \text{ GeV}/c^2 \quad (\chi^2/\text{NDF} = 293/232),$$
$$M_A^{\text{QES, GKex(05)}} = 0.991 \pm 0.011 \text{ GeV}/c^2 \quad (\chi^2/\text{NDF} = 293/232).$$

These results are well consistent within the quoted errors. Moreover,

- ❖ they are in agreement with the recent result by Bodek et al.

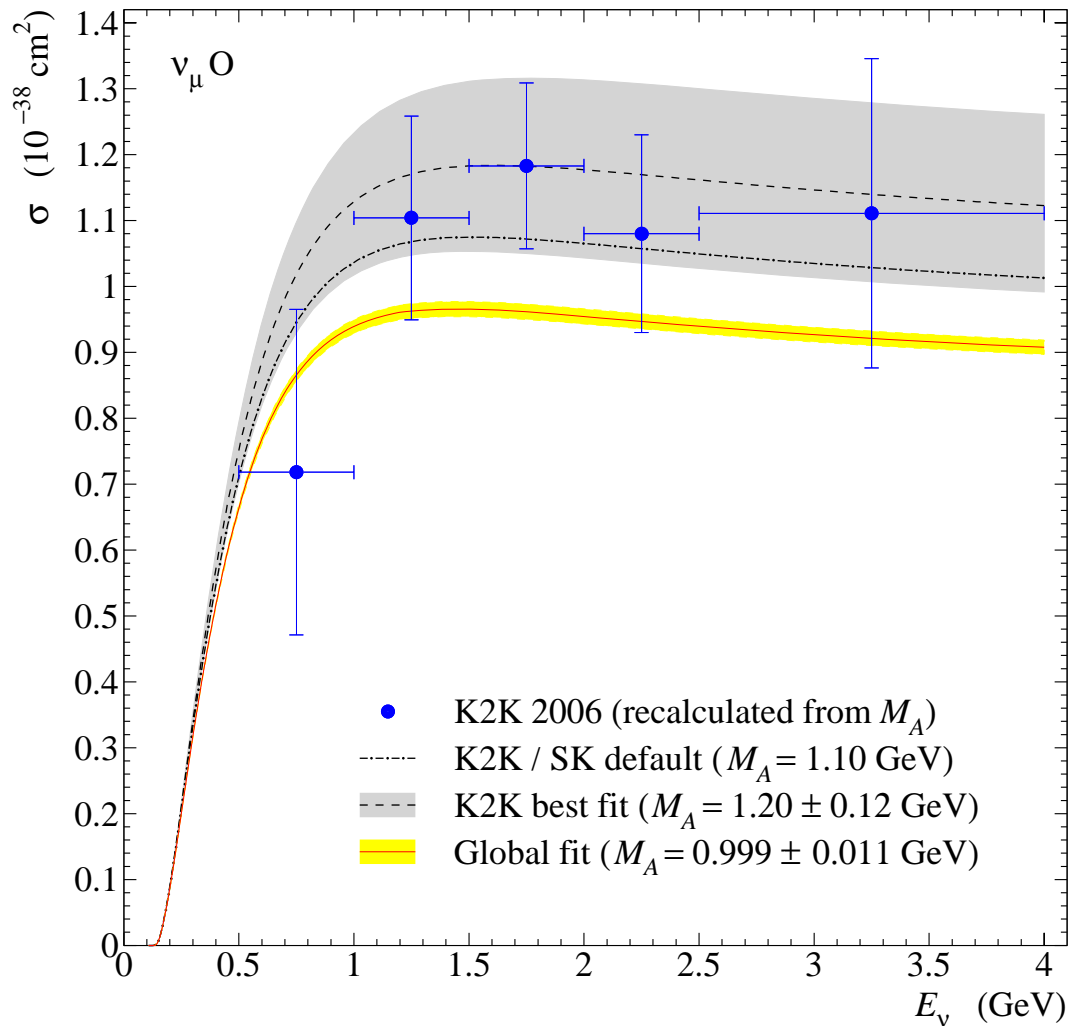
$$M_A^{\text{QES, BBBA}} = 1.014 \pm 0.014 \text{ GeV}/c^2;$$

- ❖ are compatible (being slightly below) with the values of  $M_A$  obtained recently in the high statistics **NOMAD** experiment with **carbon target** (**yet unpublished!**)

$$M_A^{\text{QES, NOMAD}}(\nu) = 1.05 \pm 0.06 \text{ GeV}/c^2, \quad M_A^{\text{QES, NOMAD}}(\bar{\nu}) = 1.06 \pm 0.13 \text{ GeV}/c^2;$$

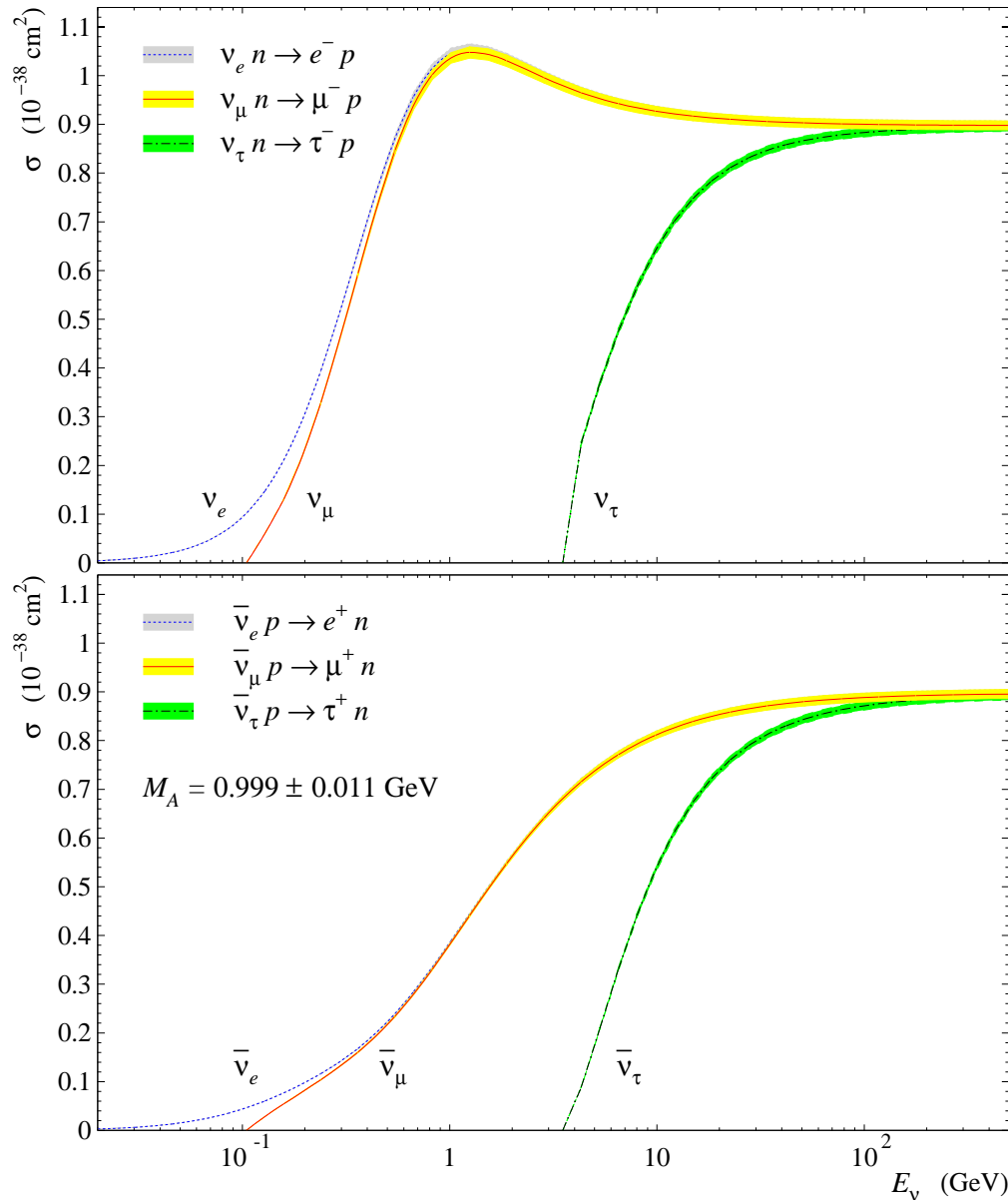
- ❖ are in a conflict with the output of two recent experiments **K2K** (**water target**) and **MiniBooNE** (**carbon target**):

$$M_A^{\text{QES, K2K}}(\nu) = 1.20 \pm 0.20 \text{ GeV}/c^2, \quad M_A^{\text{QES, MiniBooNE}}(\nu) = 1.23 \pm 0.20 \text{ GeV}/c^2.$$



The significant systematic discrepancy is clearly seen. Note that the K2K Collaboration does not consider their result for each energy bin as a *measurement*, but rather a *consistency test*.

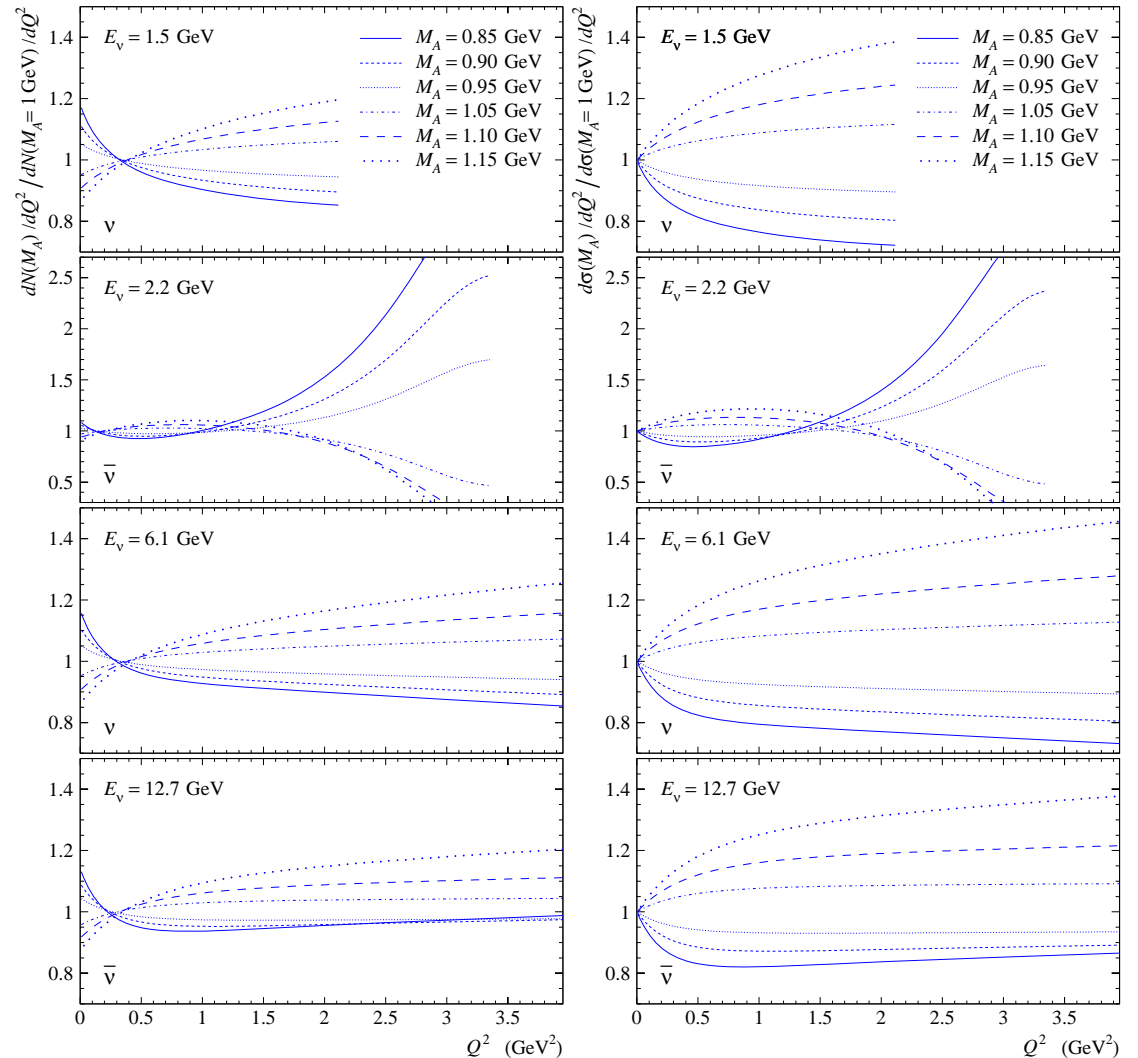
Comparison between the QES  $\nu_\mu$  cross sections per neutron bound in oxygen, evaluated with several values of the axial mass. The solid curve with narrow band is calculated with our best fit value of  $M_A$ ; the dashed curve with wide band corresponds to the K2K extraction of  $M_A$ ; the dash-dotted curve is calculated with the current K2K/SKI default ( $M_A^{\text{SK}} = 1.1 \text{ GeV}/c^2$ ). The points show the K2K cross section reconstructed from the best-fit values of  $M_A$  extracted for the five energy bins.

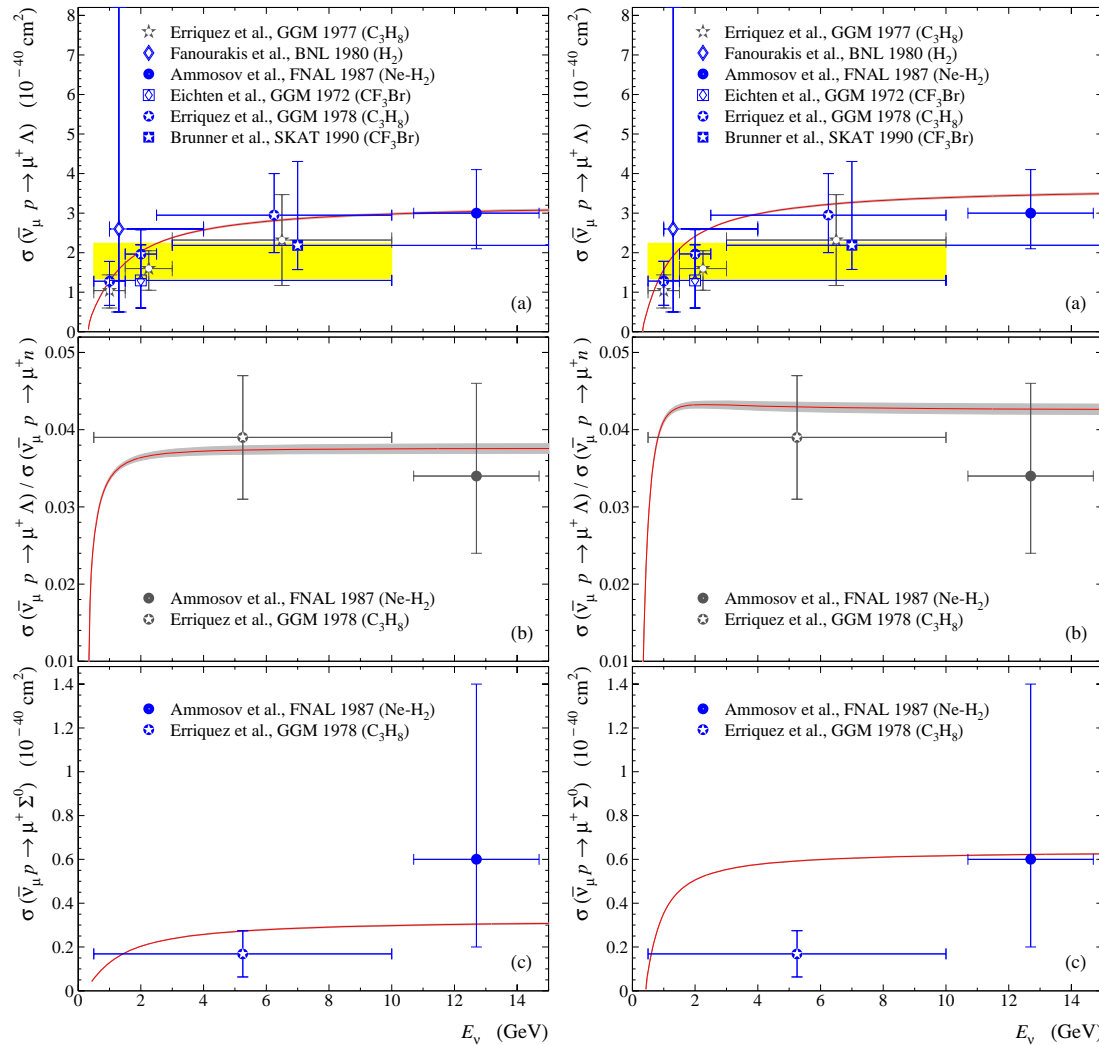


A comparison of the total QES cross sections for  $\nu_e$ ,  $\nu_\mu$ ,  $\nu_\tau$ ,  $\bar{\nu}_e$ ,  $\bar{\nu}_\mu$ , and  $\bar{\nu}_\tau$  interactions with free nucleons, calculated with the obtained best-fit value of  $M_A = 0.999 \pm 0.011 \text{ GeV}/c^2$  by using the BBBA(07) model for vector form factors. The shaded bands show the uncertainty due to the  $1\sigma$  error in  $M_A$ .

## Adds

The  $Q^2$  distributions  $dN/dQ^2$  and differential cross sections  $d\sigma/dQ^2$  vs.  $Q^2$  for  $\nu_\mu n$  and  $\bar{\nu}_\mu p$  QES interactions, calculated with different  $M_A$  and normalized to the corresponding quantities calculated with  $M_A = 1 \text{ GeV}/c^2$  at four fixed energies. Figure demonstrates that  $dN/dQ^2$  is generally less sensitive to variations of  $M_A$  than  $d\sigma/dQ^2$ .





The data on quasielastic hyperon production ( $\Delta Y = 1$ ) has been examined with two models for the transition vector form factors: a relativistic quark model by Finjord and Ravndal<sup>a</sup> [left panels] and a  $SU(3)$  based model recently adopted by Singh and Vicente Vacas<sup>b</sup> [right panels]. In the fit, the axial mass is assumed to be the same as in the QES form factors for  $\Delta Y = 0$ .

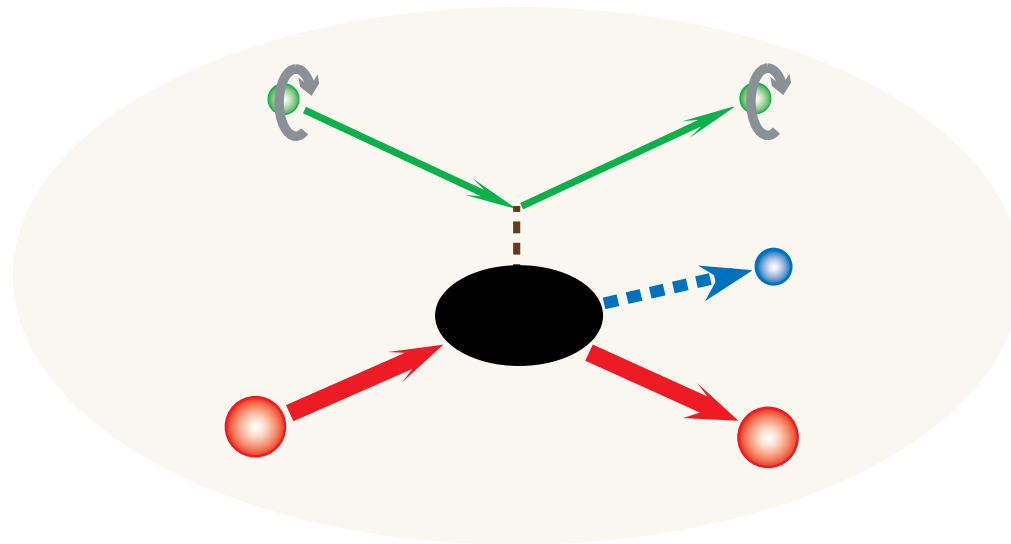
In the following analysis, we will use the second model while the poor experimental data does not permit to make a proper choice between the two models.

<sup>a</sup> J. Finjord and F. Ravndal, "Weak production of strange resonances in a relativistic quark model," Nucl. Phys. B **106**, 228 (1976).

<sup>b</sup> S. K. Singh and M. J. Vicente Vacas, "Weak quasi-elastic production of hyperons," Phys. Rev. D **74**, 053009 (2006) [arXiv:hep-ph/0606235].

# SINGLE-PION NEUTRINO PRODUCTION THROUGH BARYON RESONANCES

(Extended Rein-Sehgal model)



We adopt the famous Rein-Sehgal theory<sup>a</sup> based on the relativistic quark model by Feynman, Kislinger and Ravndal FKR.<sup>b</sup> The main feature of this model is that the region of  $W < 2.0$  GeV is covered and 18 lower  $\Delta$  and  $N$  resonances are included. The interference between the resonances with the same spin and orbital angular momentum is also taken into account.

The following changes have been made in Extended RS model (ExRS from here on).<sup>c</sup>

- ❖ The final lepton mass corrections have been properly included into the kinematics as well as into the leptonic currents. It was shown that the dynamic mass correction is very important for the  $\nu_\tau$  and  $\bar{\nu}_\tau$  induced single-pion production but, for the  $\nu_\mu$  and  $\bar{\nu}_\mu$  induced reactions it is typically at the few per cent level or less that is almost negligible in comparison with the kinematic mass corrections and with the intrinsic uncertainties of the RS model.
- ❖ The parameters of the RS model were updated according to the most recent data.
- ❖ A more accurate integration algorithm has been implemented.

---

<sup>a</sup>D. Rein and L. Sehgal, “Neutrino excitation of baryon resonances and single pion production,” *Annals Phys.* **133** (1981) 79–153 ([RS] from here on); see also D. Rein, “Angular distribution in neutrino-induced single pion production processes,” *Z. Phys. C* **35** (1987) 43–64.

<sup>b</sup>R. P. Feynman, M. Kislinger and F. Ravndal, “Current matrix elements from a relativistic quark model,” *Phys. Rev. D* **3** (1971) 2706–2732.

<sup>c</sup>K. S. Kuzmin *et al.*, “Lepton polarization in neutrino nucleon interactions,” *Mod. Phys. Lett.* **A 19** (2004) 2815–2829 [arXiv:hep-ph/0312107]; K. S. Kuzmin *et al.*, “Extended Rein-Sehgal model for tau lepton production,” *Nucl. Phys. B (Proc. Suppl.)* **139** (2005) 158–161 [arXiv:hep-ph/0408106].

Table 1: Nucleon resonances with masses below 2 GeV according to PDG

1	2	3	4	5	6	7	8
✓	$P_{11}(1440)$	$[56, 0^+]_2$	****	1430–1470	250–450 (350)	60–70 (0.65)	+
✓	$D_{13}(1520)$	$[70, 1^-]_1$	****	1515–1530	110–135 (120)	50–60 (0.56)	–
✓	$S_{11}(1535)$	$[70, 1^-]_1$	****	1520–1555	100–200 (150)	35–55 (0.45)	–
✓	$S_{11}(1650)$	$[70, 1^-]_1$	****	1640–1680	145–190 (150)	55–90 (0.60)	+
✓	$D_{15}(1675)$	$[70, 1^-]_1$	****	1670–1685	140–180 (150)	40–50 (0.35)	+
✓	$F_{15}(1680)$	$[56, 2^+]_2$	****	1675–1690	120–140 (130)	60–70 (0.62)	+
✓	$D_{13}(1700)$	$[70, 1^-]_1$	***	1650–1750	50–150 (100)	5–15 (0.10)	–
✓	$P_{11}(1710)$	$[70, 0^+]_2$	***	1680–1740	50–250 (100)	10–20 (0.19)	+
✓	$P_{13}(1720)$	$[56, 2^+]_2$	****	1650–1750	100–200 (150)	10–20 (0.19)	+
	$P_{13}(1900)$		**	~ 1900	?	$26 \pm 6$	
✓	$F_{17}(1990)$	$[70, 2^+]_2$	**	~ 1990	? (350)	$6 \pm 2$ (0.06)	+
✓	$P_{33}(1232)$	$[56, 0^+]_0$	****	1230–1234	115–125 (120)	> 99 (1.0)	+
✓	$P_{33}(1600)$	$[56, 0^+]_2$	***	1550–1700	250–450 (350)	10–25 (0.20)	+
✓	$S_{31}(1620)$	$[70, 1^-]_1$	****	1615–1675	120–180 (150)	20–30 (0.25)	+
✓	$D_{33}(1700)$	$[70, 1^-]_1$	****	1670–1770	200–400 (300)	10–20 (0.12)	+
	$P_{31}(1750)$		*	~ 1750	?	$8 \pm 3$	
	$S_{31}(1900)$		**	1850–1950	140–240 (200)	10–30	
✓	$F_{35}(1905)$	$[56, 2^+]_2$	****	1870–1920	280–440 (350)	5–15 (0.15)	–
✓	$P_{31}(1910)$	$[56, 2^+]_2$	****	1870–1920	190–270 (250)	15–30 (0.19)	–
✓	$P_{33}(1920)$	$[56, 2^+]_2$	***	1900–1970	150–300 (200)	5–20 (0.17)	+
	$D_{35}(1930)$		***	1920–1970	250–450 (350)	10–20	
	$D_{33}(1940)$		*	~ 1940	?	$18 \pm 12$	
✓	$F_{37}(1950)$	$[56, 2^+]_2$	****	1940–1960	290–350 (300)	35–40 (0.40)	+

## Explanation to Table 1

- 1 – Tick ✓ indicates that the resonance has been included into the RS calculation (Table II in [RS]).
- 2 – Resonance symbol  $L_{2I,2J}(M_i)$ , where  $L = S, D, F, P$ , the labels  $I$  and  $J$  indicate the isospin and spin, respectively, and  $M_i$  is the central mass.
- 3 – FKR relativistic quark model assignment in terms of the flavor-spin  $SU(6)$  basis  $[D, L^P]_N$ , where  $D$  is the dimensionality of the  $SU(6)$  representation,  $L$  is the total quark orbital angular momentum,  $P$  is the total parity and  $N$  is the number of quanta of excitation.
- 4 – Resonance status according to PDG'2004:
  - \*\*\*\* existence is certain, and properties are at least fairly well explored;
  - \*\*\* existence ranges from very likely to certain, but further confirmation is desirable and/or quantum numbers, branching fractions, etc. are not well determined
  - \*\* evidence of existence is only fair;
  - \* evidence of existence is poor.
- 5 – Resonance mass  $M_i$  range (in MeV).
- 6 – Breit-Wigner width  $\Gamma_i^0$  range and, in parentheses, its mean value (in MeV).
- 7 – Branching ratio of the resonance decay into the  $N\pi$  state (in %) and, in parentheses, the selected elasticity,  $\chi_i$  (see Eq. (5)).
- 8 – The pure decay sign,  $\text{sign}(N_i^*)$ , involved into Eq. (5) (as is explained in [RS]).

## Isospin structure of the amplitudes

Within the ExRS model, the elements of the polarization density matrix may be written as the superpositions of the partial cross sections<sup>a</sup>  $\sigma_L^{\lambda\lambda'}$ ,  $\sigma_R^{\lambda\lambda'}$  and  $\sigma_S^{\lambda\lambda'}$ :

$$\rho_{\lambda\lambda'} = \frac{\Sigma_{\lambda\lambda'}}{\Sigma_{++} + \Sigma_{--}}, \quad \Sigma_{\lambda\lambda'} = \sum_{i=L,R,S} c_i^\lambda c_i^{\lambda'} \sigma_i^{\lambda\lambda'},$$

and the differential cross section is given by

$$\frac{d^2\sigma}{dQ^2 dW^2} = \frac{G_F^2 \cos^2 \theta_C Q^2}{2\pi^2 M |\mathbf{q}|^2} (\Sigma_{++} + \Sigma_{--}).$$

The partial cross sections are found to be the bilinear superpositions of the reduced amplitudes for producing a  $N\pi$  final state with allowed isospin by a charged isovector current. For  $\nu$  induced reactions

$$\sigma_{L,R}^{\lambda\lambda'} = \frac{\pi W}{2M} \left( A_{\pm 3}^\lambda A_{\pm 3}^{\lambda'} + A_{\pm 1}^\lambda A_{\pm 1}^{\lambda'} \right), \quad \sigma_S^{\lambda\lambda'} = \frac{\pi M |\mathbf{q}|^2}{2WQ^2} \left( A_{0+}^\lambda A_{0+}^{\lambda'} + A_{0-}^\lambda A_{0-}^{\lambda'} \right).$$

Due to charge symmetry similar equations hold for charge conjugated  $\bar{\nu}$  induced reactions with the interchange  $L \leftrightarrow R$ .

---

<sup>a</sup>We use the same definitions and (almost) similar notation as in [RS].

The amplitudes  $A_{\varkappa}^{\lambda}$  (with  $\varkappa = \pm 3, \pm 1$  or  $0\pm$ ) for neutrino induced reactions are defined by

$$A_{\varkappa}^{\lambda} (p\pi^{+}) = \sqrt{3} \sum_{(I=3/2)} a_{\varkappa}^{\lambda} (N_3^{*+}),$$

$$A_{\varkappa}^{\lambda} (p\pi^{0}) = \sqrt{\frac{2}{3}} \sum_{(I=3/2)} a_{\varkappa}^{\lambda} (N_3^{*+}) - \sqrt{\frac{1}{3}} \sum_{(I=1/2)} a_{\varkappa}^{\lambda} (N_1^{*+}),$$

$$A_{\varkappa}^{\lambda} (n\pi^{+}) = \sqrt{\frac{1}{3}} \sum_{(I=3/2)} a_{\varkappa}^{\lambda} (N_3^{*+}) + \sqrt{\frac{2}{3}} \sum_{(I=1/2)} a_{\varkappa}^{\lambda} (N_1^{*+}).$$

Here  $\varkappa = \pm 3, \pm 1$  or  $0\pm$  and only those resonances are allowed to interfere which have the same spin and orbital angular momentum as is in the following typical example describing the  $n\pi^{+}$  final state:

$$\begin{aligned} 3A_{\varkappa}^{\lambda} A_{\varkappa}^{\lambda'} (n\pi^{+}) &= \left[ \sum a_{\varkappa}^{\lambda} (S_{31}^{+}) + \sqrt{2} \sum a_{\varkappa}^{\lambda} (S_{11}^{+}) \right] \left[ \sum a_{\varkappa}^{\lambda'} (S_{31}^{+}) + \sqrt{2} \sum a_{\varkappa}^{\lambda'} (S_{11}^{+}) \right] \\ &+ \sum_{j=1,3} \left[ \sum a_{\varkappa}^{\lambda} (P_{3j}^{+}) + \sqrt{2} \sum a_{\varkappa}^{\lambda} (P_{1j}^{+}) \right] \left[ \sum a_{\varkappa}^{\lambda'} (P_{3j}^{+}) + \sqrt{2} \sum a_{\varkappa}^{\lambda'} (P_{1j}^{+}) \right] \\ &+ \sum_{j=3,5} \left[ \sum a_{\varkappa}^{\lambda} (D_{3j}^{+}) + \sqrt{2} \sum a_{\varkappa}^{\lambda} (D_{1j}^{+}) \right] \left[ \sum a_{\varkappa}^{\lambda'} (P_{3j}^{+}) + \sqrt{2} \sum a_{\varkappa}^{\lambda'} (P_{1j}^{+}) \right] \\ &+ \sum_{j=5,7} \left[ \sum a_{\varkappa}^{\lambda} (F_{3j}^{+}) + \sqrt{2} \sum a_{\varkappa}^{\lambda} (F_{1j}^{+}) \right] \left[ \sum a_{\varkappa}^{\lambda'} (P_{3j}^{+}) + \sqrt{2} \sum a_{\varkappa}^{\lambda'} (P_{1j}^{+}) \right]. \end{aligned}$$

Any amplitude  $a_{\mathcal{Z}}^{\lambda} (N_i^{*+})$  referring to a single resonance  $N_i^{*+}$  consists of two factors which describe the production and subsequent decay of the resonance  $N_i^{*+}$ :

$$a_{\mathcal{Z}}^{\lambda} (N_i^{*}) = f_{\mathcal{Z}}^{\lambda} (\nu N \rightarrow N_i^{*}) \eta(N_i^{*} \rightarrow N\pi).$$

The decay amplitudes  $\eta(N_i^{*} \rightarrow N\pi)$  can be split into three factors:

$$\eta(N_i^{*} \rightarrow N\pi) = \text{sign}(N_i^{*}) \sqrt{\chi_i} \eta_{BW}^{(i)}(W), \quad (5)$$

irrespective of isospin, charge or helicity. Here

$\text{sign}(N_i^{*})$  is the decay sign for resonance  $N_i^{*}$  (Table III of [RS]),

$\chi_i$  is the elasticity of the resonance taking care of the branching ratio into the  $\pi N$  final state,

$\eta_{BW}^{(i)}(W)$  is the properly normalized Breit-Wigner term with the running width specified by the  $\pi N$  partial wave from which the resonance arises; it is given by

$$\eta_{BW}^{(i)}(W) = \sqrt{\frac{\Gamma_i(W)}{2\pi N_i}} \left[ \frac{1}{W - M_i + i\Gamma_i(W)/2} \right],$$

with

$$\Gamma_i(W) = \Gamma_i^0 \left[ \frac{p_{\pi}^{*}(W)}{p_{\pi}^{*}(M_{\Delta})} \right]^{2L+1} \quad \text{and} \quad N_i = \frac{1}{2\pi} \int \frac{\Gamma_i(W) dW}{(W - M_i)^2 + \Gamma_i^2(W)/4}.$$

## Vector and axial transition form factors

The transition form factors are assumed to have the form

$$G^{V,A}(Q^2) = \left(1 + \frac{Q^2}{4M^2}\right)^{1/2-n} \left(1 + \frac{Q^2}{M_{V,A}^2}\right)^{-2} \quad (6)$$

with the “standard” value of the vector mass  $M_V = 0.84 \text{ GeV}/c^2$ . The axial mass  $M_A$  will be a free parameter.<sup>a</sup> The parameter  $n$  in the first (“ad hoc”) factor of Eq. (6) is the number of oscillator quanta present in the final resonance.

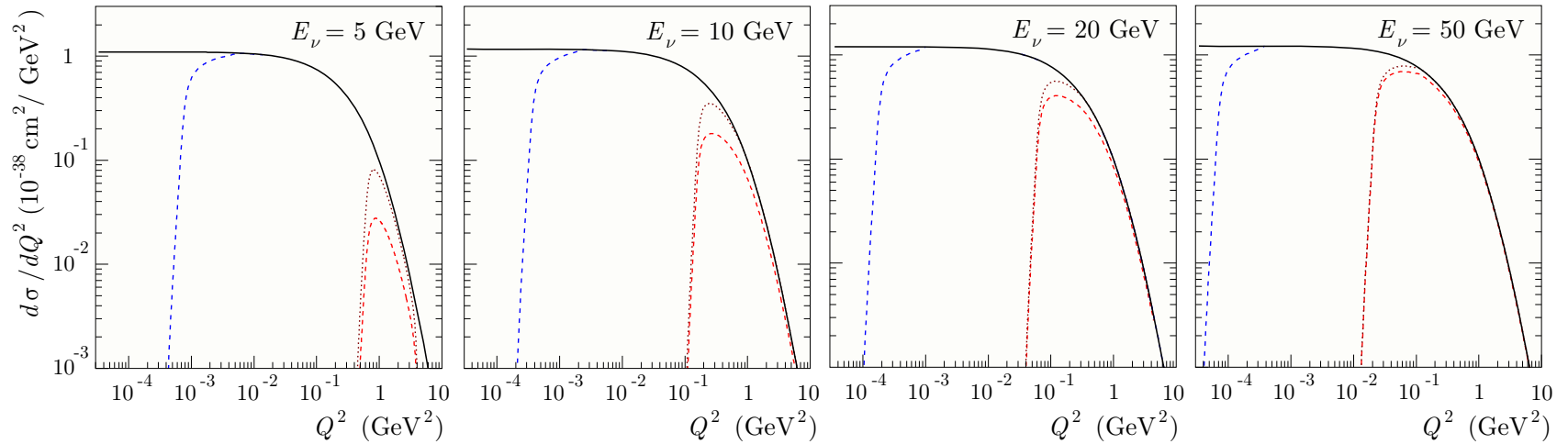
## Resonance set

- ◆ In our calculations, we use the same set of 18th baryon resonances with masses below  $2 \text{ GeV}/c^2$  as in [RS] but with all relevant parameters updated according to the most recent RPP.<sup>b</sup> as is shown in Table 1 (next slide).
- ◆ The factors which were estimated in [RS] numerically are corrected by using the new data and a more accurate integration algorithm.

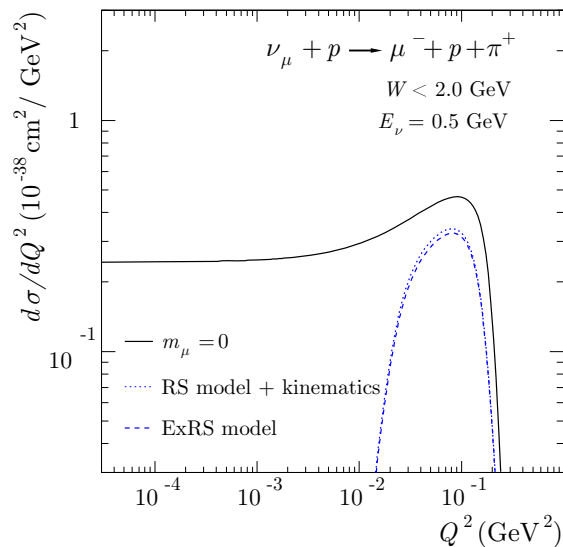
---

<sup>a</sup>In [RS] it has been taken to be  $0.95 \text{ GeV}/c^2$ .

<sup>b</sup>W. M. Yao *et al.* (Particle Data Group), “Review of particle physics,” J. Phys. G **33** (2006) 1–1232.



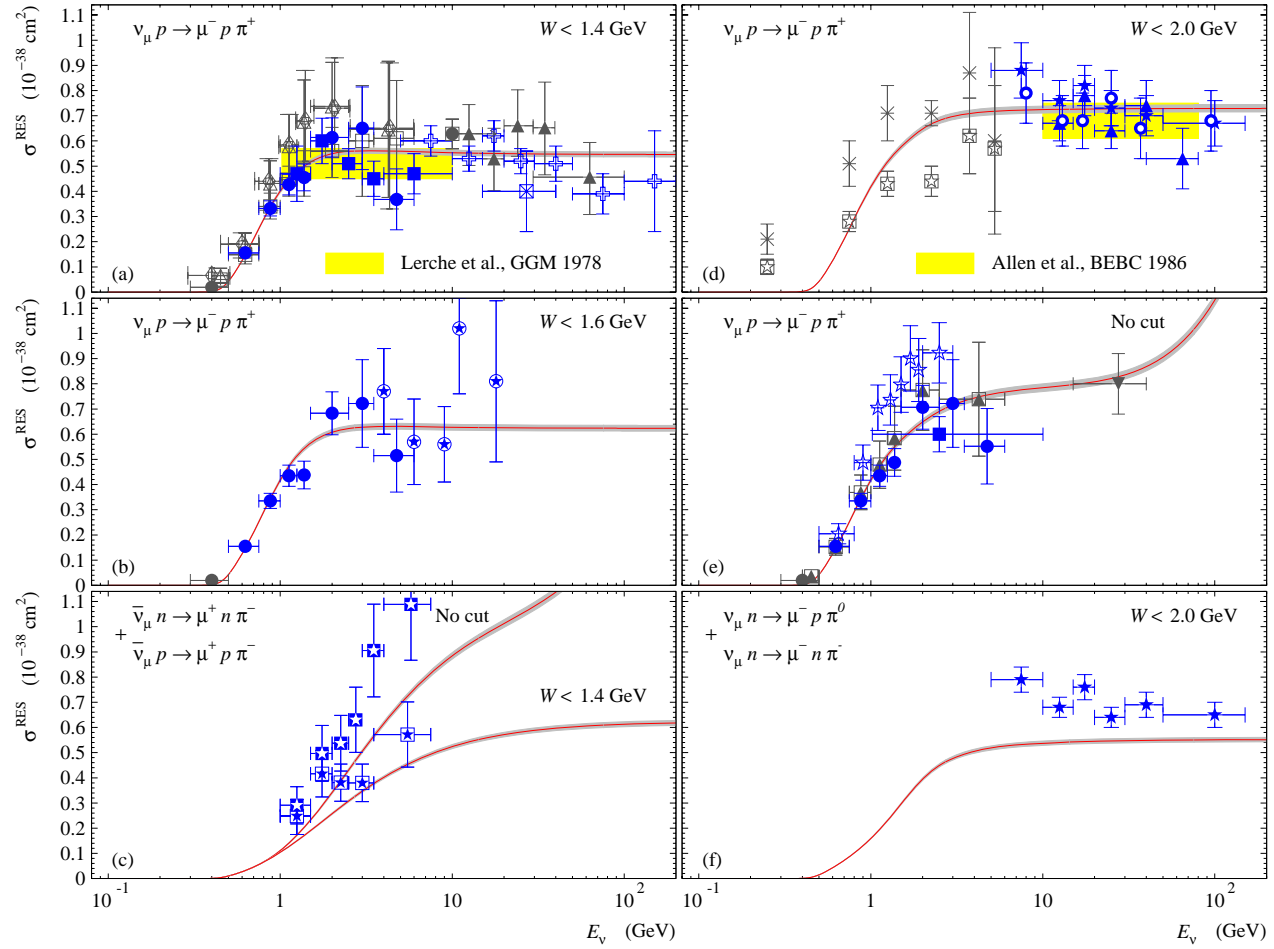
An example of the finite lepton mass effect for the  $\nu_\tau p \rightarrow \tau^- p \pi^+$  differential cross section at  $E_\nu = 5, 10, 20$  and  $50$  GeV. The phase space has been cut by the condition  $W < 2$  GeV.



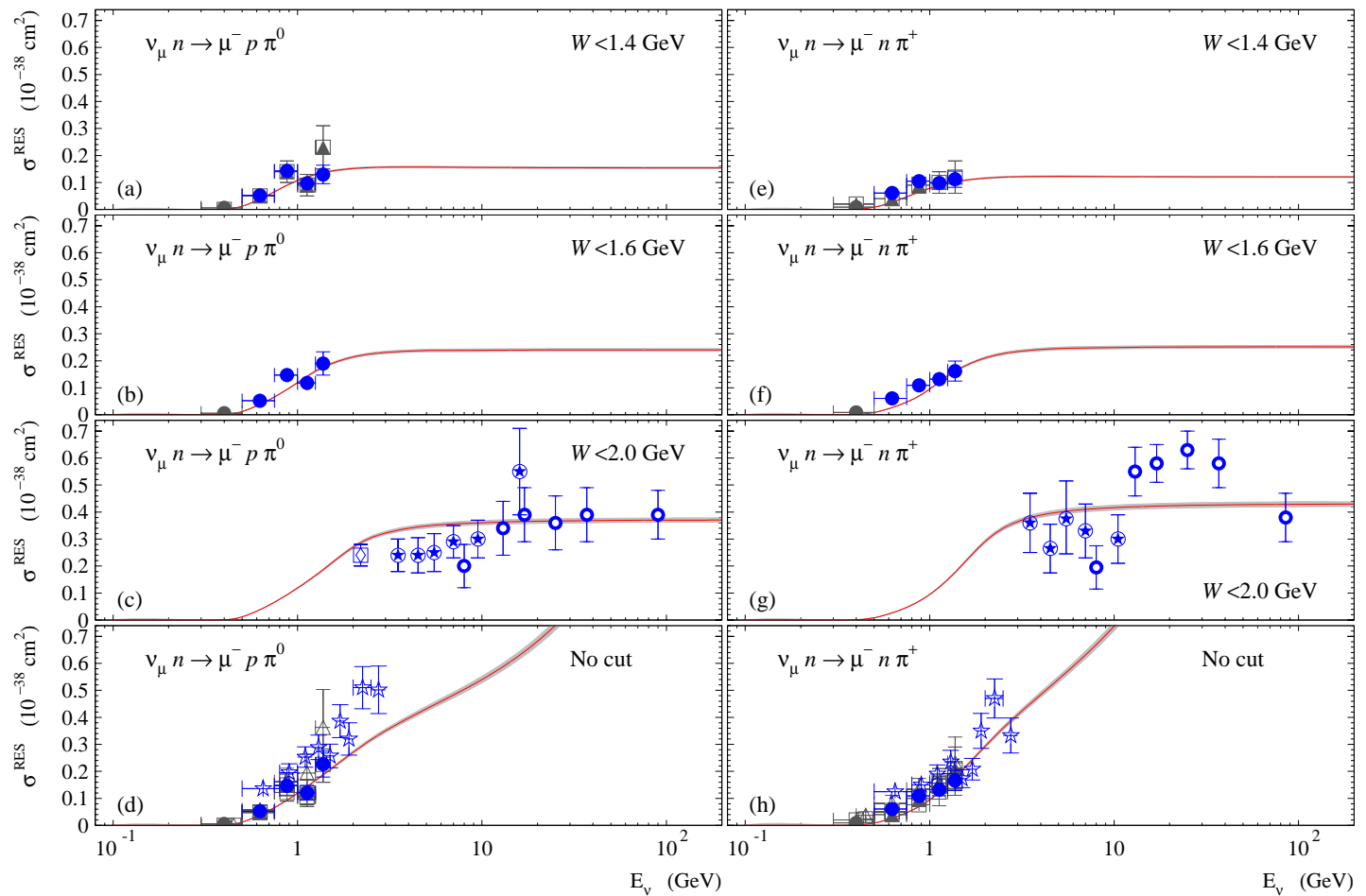
The major effect is, of course, due to the  $\tau$  lepton production threshold but the accounting for the mass in the lepton current (“dynamic correction”) gives rise to a significant additional decrease of the cross section: the effect can be as large as 300% at low neutrino energies and remains important up to rather high energies.

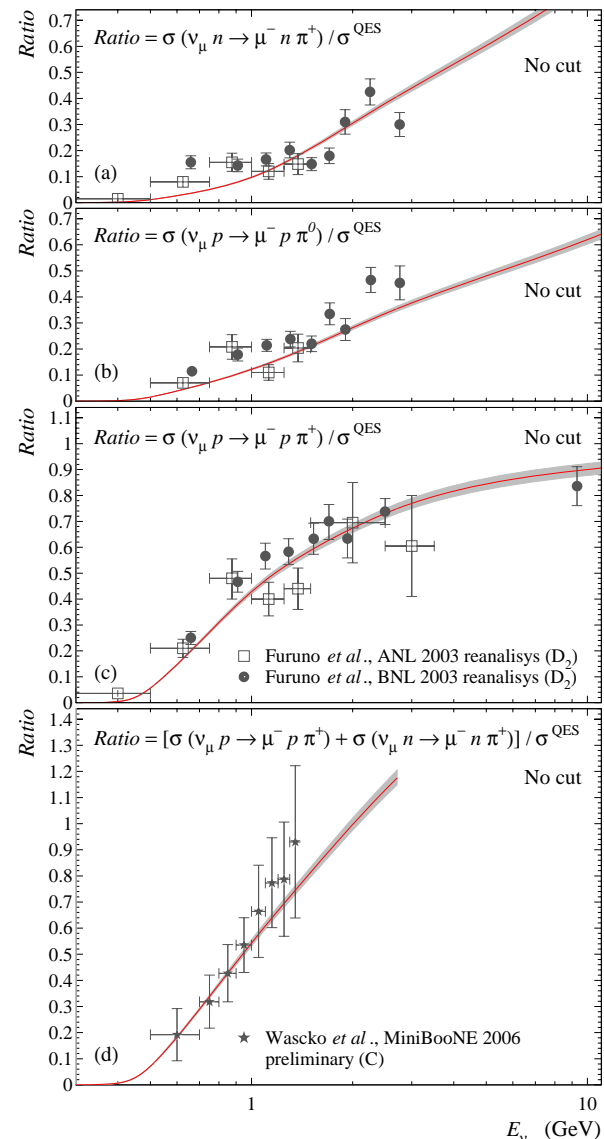
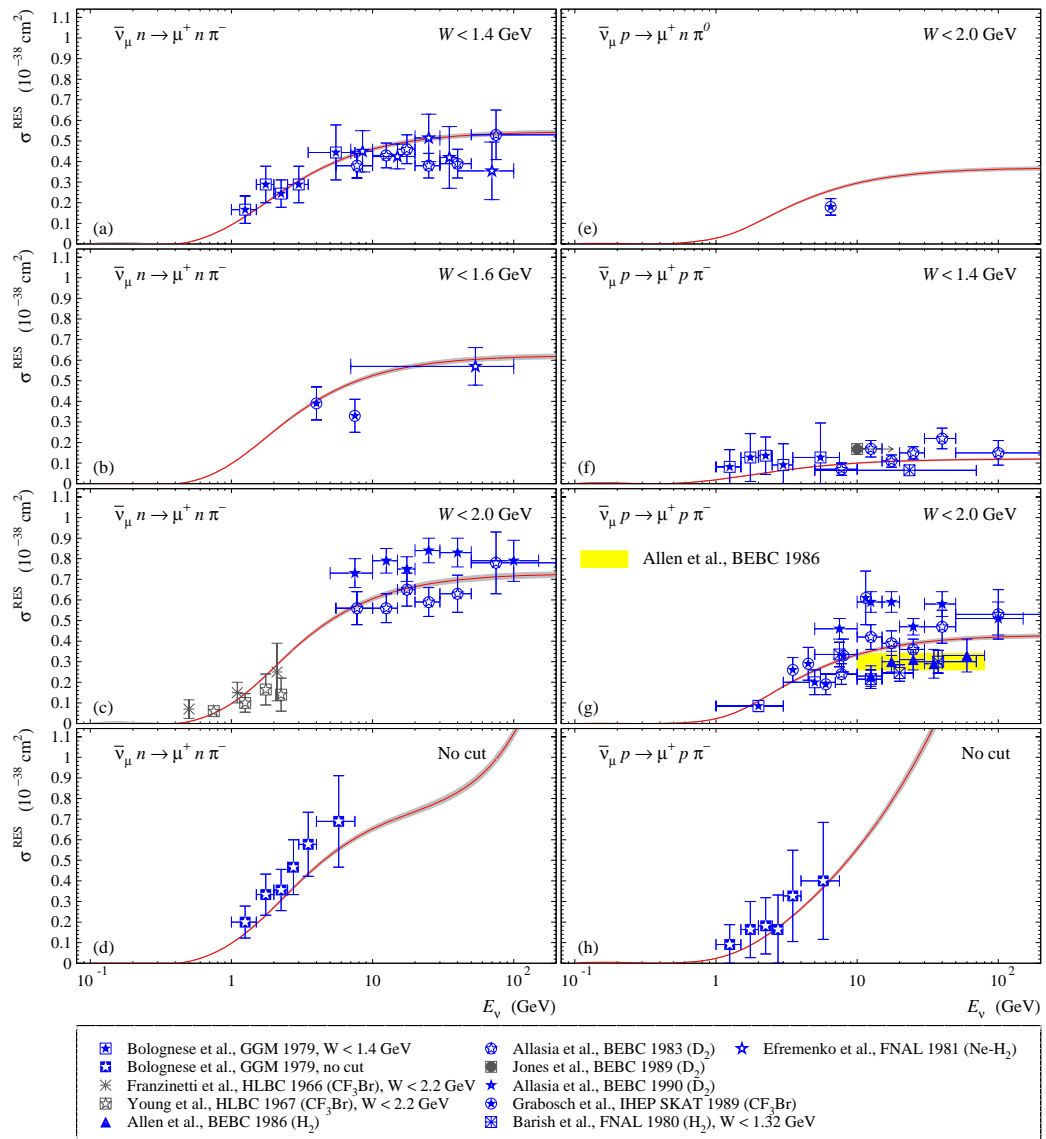
In the case of  $\nu_\mu p \rightarrow \mu^- p \pi^+$ , the dynamic mass correction is typically at the few per cent level or less and the purely kinematic correction for the muon mass is sufficient.

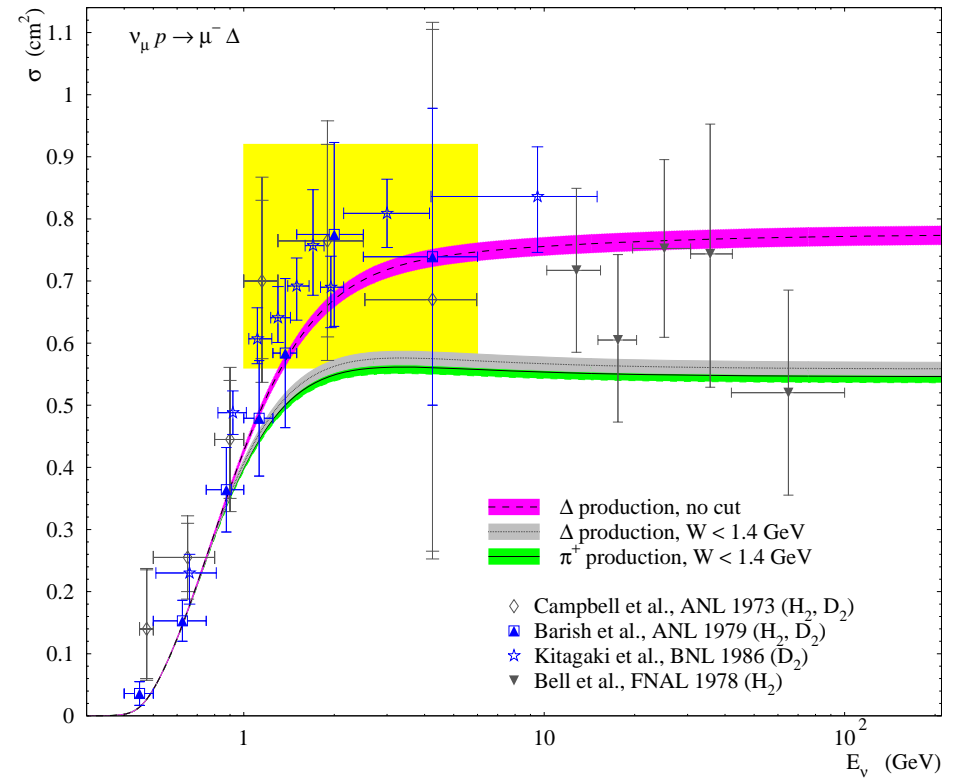
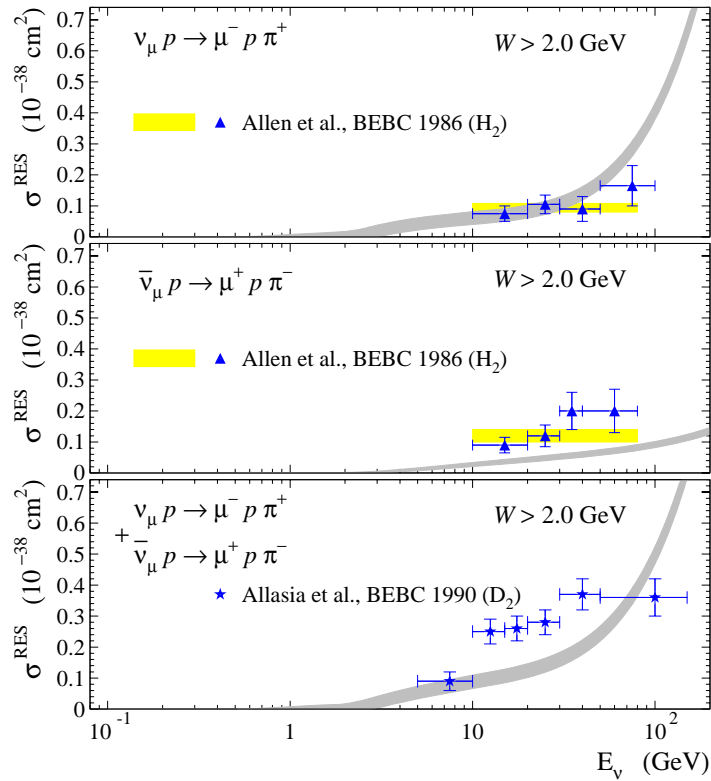
The situation is qualitatively similar for the rest  $\nu$  and  $\bar{\nu}$  induced reactions under consideration.



◊ Barish et al., ANL 1975 ( $D_2$ )	* Franzinetti et al., HLBC 1966 ( $CF_3Br$ ), $W < 2.2 \text{ GeV}$
△ Barish et al., ANL 1976 ( $H_2$ , $D_2$ )	⊠ Young et al., HLBC 1967 ( $CF_3Br$ ), $W < 2.2 \text{ GeV}$
□ Barnes et al., ANL 1978 ( $D_2$ )	■ Lerche et al., GGM 1978 ( $C_3H_8$ - $CF_3Br$ )
▲ Barish et al., ANL 1979 ( $H_2$ , $D_2$ )	⊕ Allen et al., BEBC 1980 ( $H_2$ )
● Radecky et al., ANL 1982 ( $H_2$ , $D_2$ )	▲ Allen et al., BEBC 1986 ( $H_2$ )
☆ Kitagaki et al., BNL 1986 ( $D_2$ )	■ Jones et al., BEBC 1989 ( $D_2$ )
▼ Bell et al., FNAL 1978 ( $H_2$ )	★ Allasia et al., BEBC 1990 ( $D_2$ )
▲ Ross et al., FNAL 1978 ( $H_2$ )	○ Barlag et al., BEBC 1984 ( $D_2$ )
⊠ Barish et al., FNAL 1980 ( $H_2$ )	⊠ Grabosch et al., IHEP SKAT 1989 ( $CF_3Br$ )
	⊠ Bolognese et al., GGM 1979 ( $C_3H_8$ - $CF_3Br$ ), $W < 1.4 \text{ GeV}$
	⊠ Bolognese et al., GGM 1979 ( $C_3H_8$ - $CF_3Br$ ), no cut







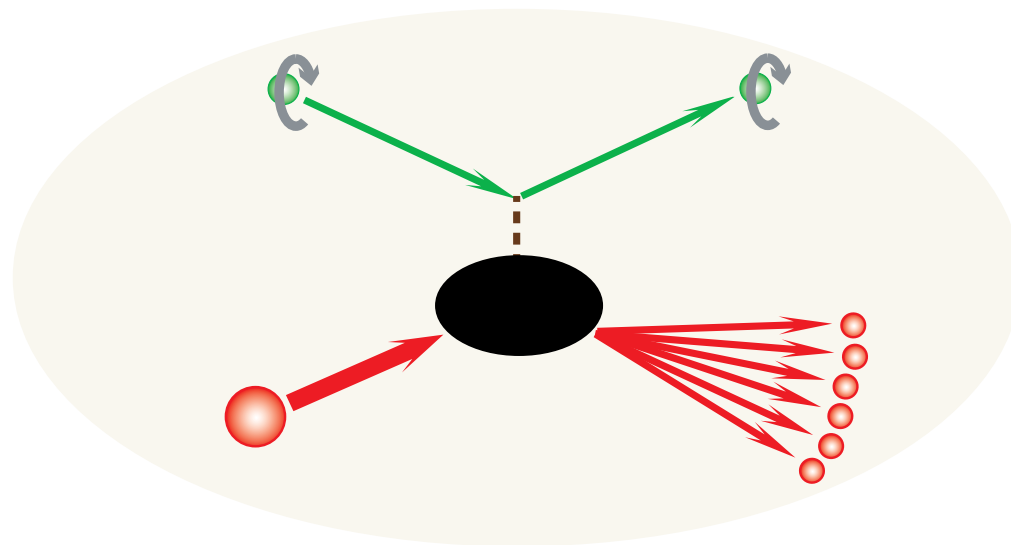
The resulting value of  $M_A$  obtained from the fit to the single-pion production data is

$$M_A^{\text{RES}} = 1.093 \pm 0.016 \text{ GeV} \quad (\chi^2/\text{NDF} = 300/228 = 1.318).$$

It should be compared with the “elastic” axial mass discussed above:

$$M_A^{\text{QES, GKex(05)}} = 0.991 \pm 0.011 \text{ GeV}/c^2 \quad \text{or} \quad M_A^{\text{QES, BBBA(07)}} = 0.999 \pm 0.011 \text{ GeV}/c^2.$$

# DEEP INELASTIC SCATTERING



The DIS CC  $\nu_\ell N$  and  $\bar{\nu}_\ell N$  ( $\ell = e, \mu, \tau$ ) differential cross section is represented by a standard set of 5 structure functions  $F_i = F_i(x, Q^2)$ <sup>a</sup>

$$\frac{d^2\sigma^{\nu(\bar{\nu})}}{dxdy} = \frac{G_F^2 M_N E}{\pi(1 + Q^2/M_W^2)^2} \sum_{i=1}^5 A_i(x, y, E) F_i(x, Q^2),$$

where  $x$ ,  $y$  and  $Q^2$  are the standard DIS kinematic variables and the coefficient functions  $A_i$  are

$$\begin{aligned} A_1 &= y \left( xy + \frac{m_\ell^2}{2M_N E} \right), \\ A_2 &= 1 - \left( 1 + \frac{M_N x}{2E} \right) y - \frac{m_\ell^2}{4E^2}, \\ A_3 &= \pm y \left[ x \left( 1 - \frac{y}{2} \right) - \frac{m_\ell^2}{4M_N E} \right], \\ A_4 &= \frac{m_\ell^2}{2M_N E} \left( y + \frac{m_\ell^2}{2M_N E x} \right), \\ A_5 &= -\frac{m_\ell^2}{M_N E}. \end{aligned}$$

---

<sup>a</sup>See, e.g., S. Kretzer and M. H. Reno, "Target mass corrections to electro-weak structure functions and perturbative neutrino cross sections," Phys. Rev. D **69** (2004) 034002 [arXiv:hep-ph/0307023].

## Structure Functions

The longitudinal SF

$$F_L = (1 + Q^2/\nu^2) F_2 - 2xF_1$$

vanishes in the collinear parton model (PM) approximation, as  $Q^2 \rightarrow \infty$  since

$$F_2^{\text{PM}} = 2xF_1^{\text{PM}} \quad (\text{Callan-Gross relation}). \quad (7)$$

In the next order in  $\alpha_s$  the structure functions  $F_2$  and  $F_L$  are related through the Altarelli-Martinelli equation:

$$F_L(x, Q^2) = \frac{4\alpha_s(Q^2)}{3\pi} \int_x^1 \frac{dy}{y} \left(\frac{x}{y}\right)^2 [F_2(y, Q^2) + C_g(y-x)G(y, Q^2)] + \mathcal{O}(\alpha_s^2).$$

Here  $xG(x, Q^2)$  is the gluon density function and

$$C_g = \begin{cases} \frac{3}{4} \sum_1^{2f} e_q^2 & \text{in lepton scattering,} \\ 3f/2 & \text{in (anti)neutrino scattering.} \end{cases}$$

In particular, for four flavors,  $C_g^{(l)} = 5/3$  and  $C_g^{(\nu)} = 6$ .

In the general case the functions  $F_1$  and  $F_2$  are related through the *measurable* structure function  $R = \sigma_L/\sigma_T$ :

$$\mathfrak{D}F_2 = 2xF_1, \quad \text{where} \quad \mathfrak{D} = \frac{1}{1+R} \left( 1 + \frac{Q^2}{\nu^2} \right). \quad (8)$$

According to Eq. (8) and the Callan-Gross relation (7),  $F_{1,2}$  and  $F_{1,2}^{\text{PM}}$  are related by

$$F_1 = (1 - a + a\mathfrak{D}) F_1^{\text{PM}}, \quad F_2 = [a + (1 - a)/\mathfrak{D}] F_2^{\text{PM}}.$$

Till the function  $a = a(x, Q^2)$  is not specified, these relations are the most general. From the exact  $\nu N$  kinematics it follows that

$$A_4 < \frac{m_\ell^2}{2M_N E} \left( 1 - \frac{m_\ell}{E} \right) < \frac{m_\ell}{2M_N} \quad \text{and} \quad |A_5| < \frac{m_\ell}{M_N}.$$

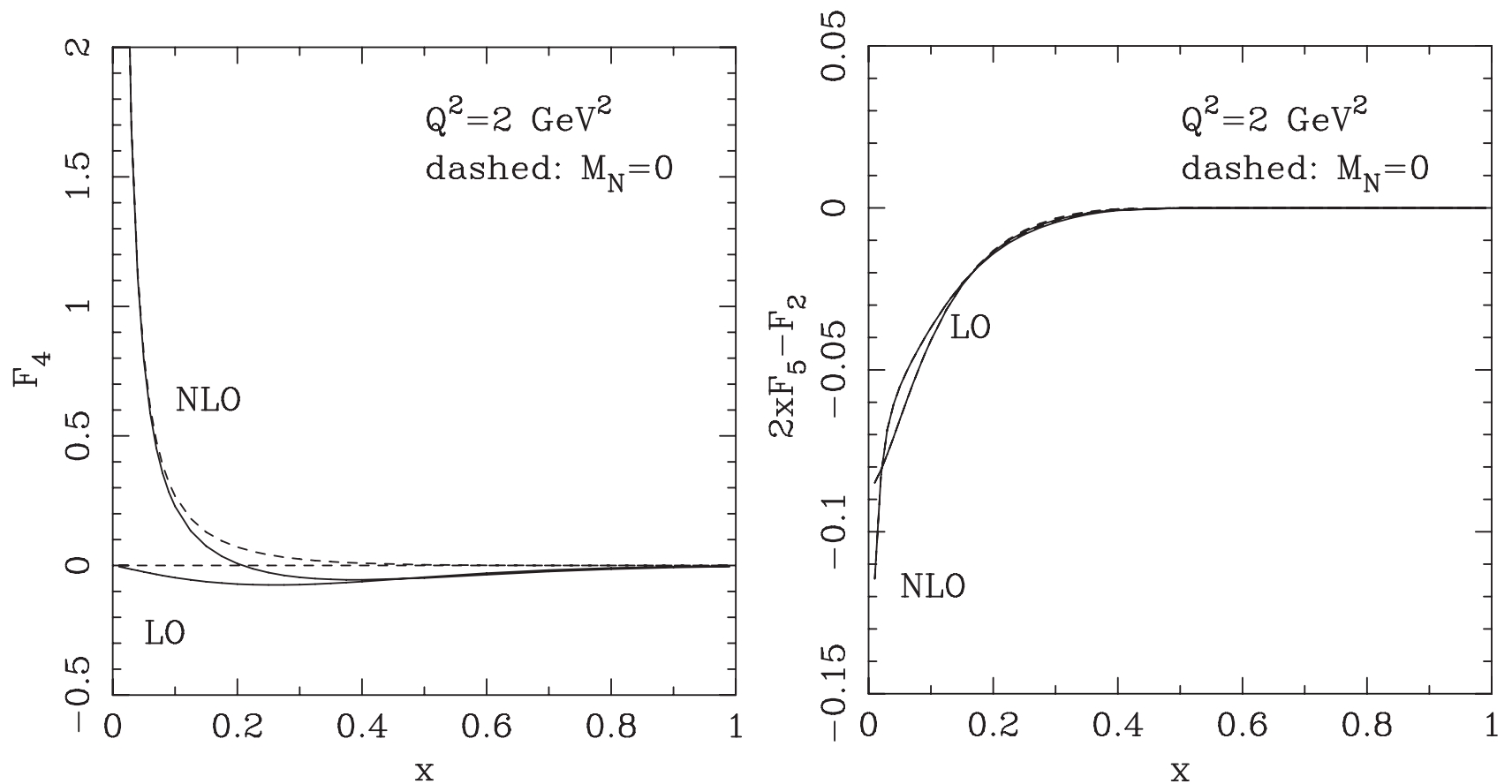
Therefore, for **electron** and **muon** neutrinos, the structure functions  $F_4$  and  $F_5$  may visibly contribute only near the reaction threshold<sup>a</sup> and can be estimated roughly, by using the approximate relations:

$$F_4 \approx \frac{1}{2} \left( \frac{F_2}{2x} - F_1 \right) = \frac{1}{2} \left( \frac{1}{\mathfrak{D}} - 1 \right) F_1 \quad \text{and} \quad F_5 \approx \frac{F_2}{2x} = \frac{F_1}{\mathfrak{D}},$$

which only valid in the PM with massless quarks.

---

<sup>a</sup>But Fermi motion ... but cutoff on  $W$  ...



The structure function  $F_4$  and the difference  $2xF_5 - F_2$  vs  $x$  at fixed  $Q^2 = 2 \text{ GeV}^2$ , evaluated from  $\overline{\text{MS}}$  QCD at LO and NLO, using the CTEQ6 PDFs. Dashed lines show the case without target mass correction.

[Taken from S. Kretzer and M. H. Reno, "Tau neutrino deep inelastic charged current interactions," Phys. Rev. D **66** (2002) 113007 [arXiv:hep-ph/0208187]. ]

There are two simplest limiting possibilities for  $a$ :

- 1:  $a = 0 \implies F_1 = F_1^{\text{PM}}, F_2 = F_2^{\text{PM}}/\mathcal{D}$  (Bodek-Yang approach);
- 2:  $a = 1 \implies F_1 = \mathcal{D}F_1^{\text{PM}}, F_2 = F_2^{\text{PM}}$  (our choice for the moment).

For the structure function  $R$  we use a combination of two up-to-date parametrizations: inside the nucleon resonance region  $1.15 < W^2 < 3.9 \text{ GeV}^2$  and  $0.3 < Q^2 < 5.0 \text{ GeV}^2$  we apply the recent precision result of the Jefferson Lab Hall C E94-110 Collaboration;<sup>a</sup> outside this region we apply the  $R_a$  version of the accurate 6-parameter fit to the world data on  $R$  proposed by the SLAC E-143 Collaboration.<sup>b</sup> The two parametrizations are sewn by a 2D B-spline in the boundary of the kinematic regions.

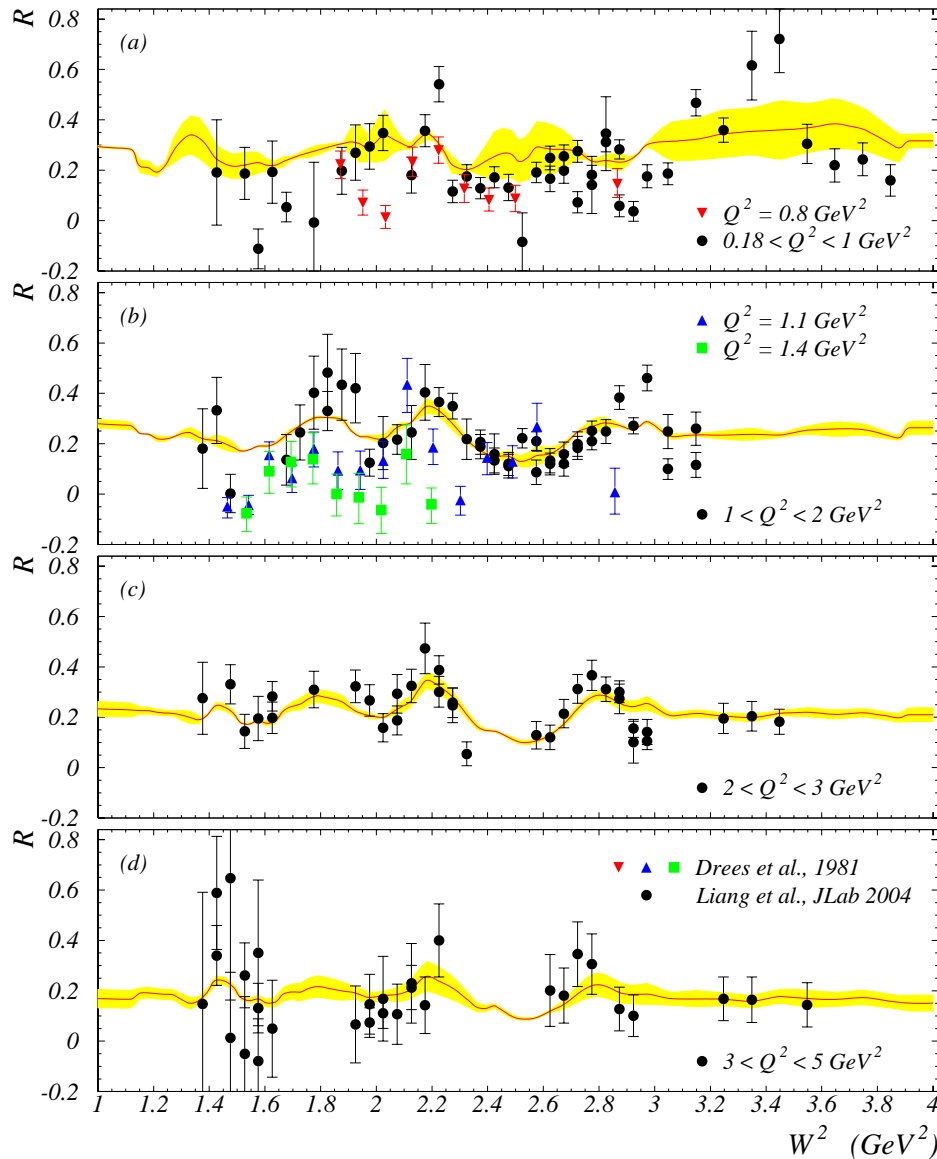
Since the JLab fit has been obtained from the data on  $ep$  scattering, we corrected it to the  $\nu N$  scattering and tested by using the Altarelli-Martinelli equation.

In fact, the difference between  $R^{(e,\mu)}$  and  $R^{(\nu,\bar{\nu})}$  is practically negligible within the relevant kinematic region below the charm production threshold and small above the threshold.

---

<sup>a</sup>Y. Liang *et al.*, “Measurements of  $R = \sigma_L/\sigma_T$  and the separated longitudinal and transverse structure functions in the nucleon resonance region,” [arXiv:nucl-ex/0410027].

<sup>b</sup>K. Abe *et al.*, “Measurements of  $R = \sigma_L/\sigma_T$  for  $0.03 < x < 0.1$  and fit to world data,” Phys. Lett. B **452** (1999) 194–200 [arXiv:hep-ex/9808028].



Parametrization by Y. Liang<sup>a</sup> of the JLab Hall C E94-110 data sewn by spline with the SLAC E-143  $R_a$  model outside the region  $1.15 < W^2 < 3.9 \text{ GeV}^2$  and  $0.3 < Q^2 < 5.0 \text{ GeV}^2$ . Also shown are the results of several earlier experiments on  $ep$  scattering in the resonance region converted to  $R$  by Dress *et al.*<sup>b</sup> for  $Q^2 = 0.8$  (a), 1.1 and 1.4  $\text{GeV}^2$  (b).

<sup>a</sup>Y. Liang, Ph. D. thesis, The American University (2003) and private communication (2005).

<sup>b</sup>J. Dress, B. Gerhardt, Ch. Gerhardt, and A. Schneider, "Determination of the longitudinal and transverse cross section in resonance electroproduction," *Z. Phys. C* **7** (1981) 183–185.

## Other important features of the model

- ◆ The PDF contributions into all structure functions are divided in the standard fashion onto “non charm production” (ncp) and “charm production” (cp):

$$q^{\text{ncp}} = q^{\text{ncp}}(x_N, Q^2) \quad \text{and} \quad q^{\text{cp}} = q^{\text{cp}}(\xi, Q^2).$$

Here

$$x_N = \frac{Q^2}{2M^2x} \left( \sqrt{1 + \frac{4M^2x^2}{Q^2}} - 1 \right) = \frac{2x}{1 + \sqrt{1 + Q^2/\nu^2}}.$$

is the Nachtmann variable and

$$\xi = x_N \left( 1 + \frac{m_c^2}{Q^2} \right) = \frac{x_N}{\lambda},$$

is the collinear limit of the light-cone variable<sup>a</sup>

$$x_F = \frac{x_N}{2} \left[ 1 + \frac{m_f^2 - m_i^2}{Q^2} + \sqrt{1 + \frac{2(m_f^2 + m_i^2 + 2k_T^2)}{Q^2} + \left( \frac{m_f^2 - m_i^2}{Q^2} \right)^2} \right],$$

with massless  $u$ ,  $d$ , and  $s$  quarks, and  $m_c = 1.3 \text{ GeV}/c^2$  is the mass of  $c$  quark.

---

<sup>a</sup> $m_i$  and  $m_f$  are the masses of the struck and final partons, and  $k_T$  is the transverse momentum of the struck parton in the Breit frame.

- ◆ The difference between  $R^{(e,\mu)}$  and  $R^{(\nu,\bar{\nu})}$  is only important for the charm production contributions. Hence we neglect it below the charm production threshold and apply the corresponding (small) correction above the threshold.
- ◆ We examine four NLO QCD models for parton density functions (PDF):
  1. GRV 98<sup>b</sup> [ $0.8 \lesssim Q^2 < 10^6 \text{ GeV}^2, x > 10^{-8}$ ],
  2. MRST 04<sup>c</sup> [ $1.25 \lesssim Q^2 < 10^7 \text{ GeV}^2, x > 10^{-5}$ ],
  3. CTEQ 6D<sup>d</sup> [ $0.05 \lesssim Q^2 < 10^8 \text{ GeV}^2, x > 10^{-6}$ ],
  4. CTEQ 6.5M<sup>e</sup> [ $0.05 \lesssim Q^2 < 10^8 \text{ GeV}^2, x > 10^{-6}$ ].

---

<sup>b</sup>M. Glück, E. Reya, and A. Vogt, “Dynamical parton distributions revisited,” *Eur. Phys. J. C* **5** (1998) 461–470 [arXiv:hep-ph/9806404].

<sup>c</sup>A. D. Martin, R. G. Roberts, W. J. Stirling, and R. S. Thorne, “Uncertainties of predictions from parton distributions. II: Theoretical errors,” *Eur. Phys. J. C* **35** (2004) 325–348 [arXiv:hep-ph/0308087]; R. S. Thorne, A. D. Martin, W. J. Stirling, and R. G. Roberts, “Update of MRST parton distributions,” arXiv:hep-ph/0407311.

<sup>d</sup>J. Pumplin *et al.*, “New generation of parton distributions with uncertainties from global QCD analysis,” *JHEP*07 (2002) 012 [arXiv:hep-ph/0201195]; D. Stump *et al.*, “Inclusive jet production, parton distributions, and the search for new physics,” *JHEP*10 (2003) 046 [arXiv:hep-ph/0303013]; S. Kretzer *et al.*, “CTEQ 6 parton distributions with heavy quark mass effects,” *Phys. Rev. D*69 (2004) 114005 [arXiv:hep-ph/0307022]; F. Olness *et al.*, “Neutrino dimuon production and strangeness asymmetry of the nucleon,” *Eur. Phys. J. C* **40** (2005) 145–156 [arXiv:hep-ph/0312323].

<sup>e</sup>W. K. Tung *et al.*, “Heavy quark mass effects in deep inelastic scattering and global QCD analysis,” *JHEP* **02** (2007) 053 [arXiv:hep-ph/0611254]; J. Pumplin, H. L. Lai, and W. K. Tung, “The charm parton content of the nucleon,” *Phys. Rev. D* **75** (2007) 054029 [arXiv:hep-ph/0701220].

In order to extrapolate the PDFs to low  $Q^2$  and  $x$  we have to apply an phenomenological procedure. Namely, for the region  $Q^2 < Q_f^2$ , we are testing the following simplest possibilities which can be written symbolically as

$$\mathbf{1p:} \quad q(x, Q^2) \longmapsto q(xQ_f^2/Q^2, Q_f^2),$$

$$\mathbf{2p:} \quad q(x, Q^2) \longmapsto q(xQ_f^2/Q^2, Q_f^2) \left[ \frac{Q^2}{Q^2 + Q_1^2} \right] [\lim_{Q^2 \rightarrow 0} F_2 = 0],$$

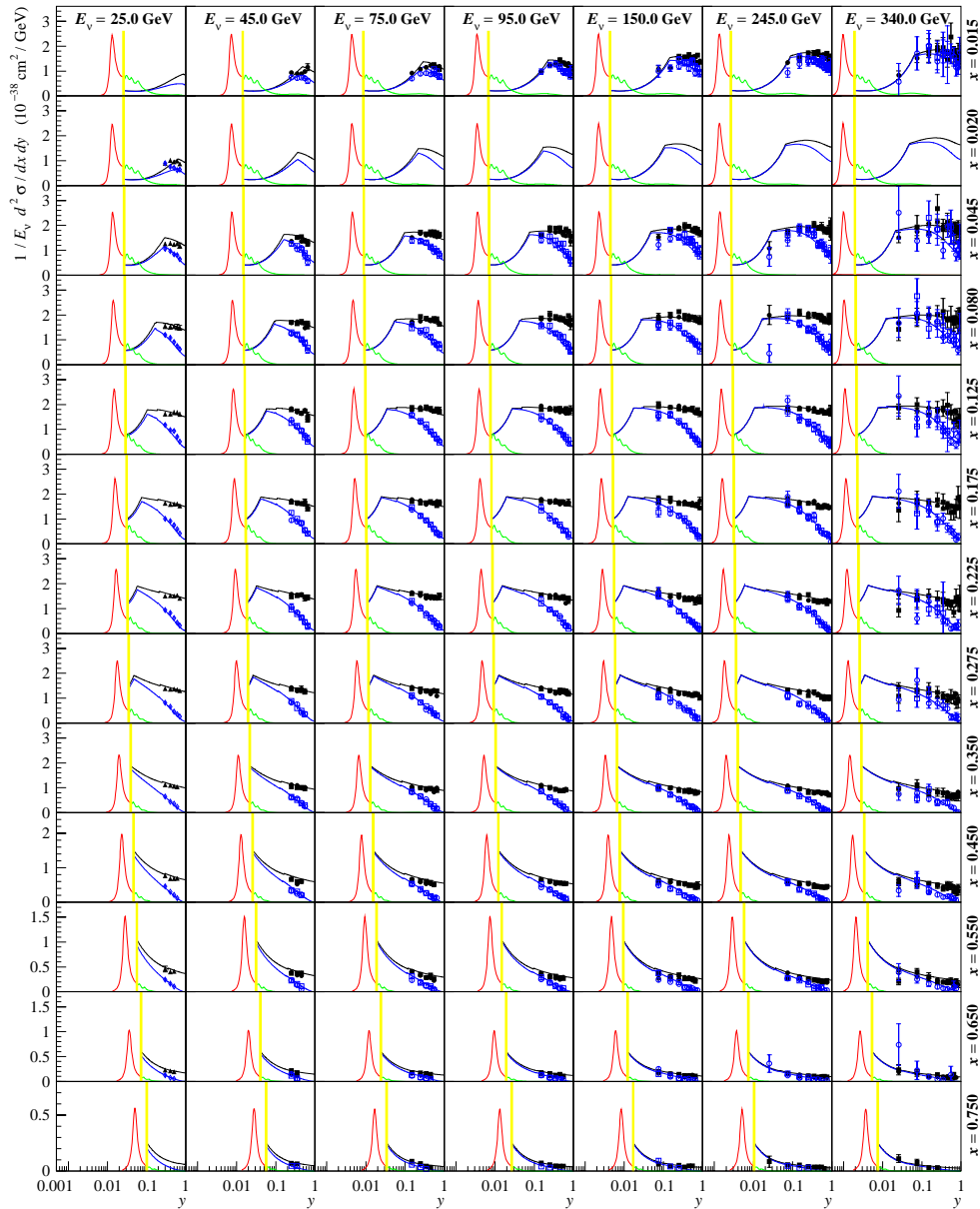
$$\mathbf{4p:} \quad q(x, Q^2) \longmapsto q(xQ_f^2/Q^2, Q_f^2) \left[ \frac{Q^2}{Q^2 + Q_1^2} + \frac{Q_2^2}{Q^2 + Q_3^2} \right] [\lim_{Q^2 \rightarrow 0} F_2 = \text{const} \geq 0],$$

where the unknown parameters  $Q_1^2$ ,  $Q_2^2$ ,  $Q_3^2$ , and  $Q_f^2$  are subject of adjusting to the measured double differential (anti)neutrino-nucleon cross sections.

In a sense, the “receipts” **2p** and **4p** empirically account for the **high-twist effect** while the **1p** receipt simply extrapolates the structure functions outside the kinematic region available in the PDF models under consideration.

Our analysis shows that the uncertainty introduced by these receipts is almost negligible in comparison with the difference in the PDF models.

Below we'll illustrate our analyses mainly with the simplest **GRV98 (1p)** PDF model.



RES and DIS contributions to the double differential cross sections (divided by energy) for  $\nu_\mu$  and  $\bar{\nu}_\mu$  scattering off isoscalar nucleon, vs.  $E_\nu$ ,  $x$ , and  $y$ . The DIS contribution is calculated using GRV 98 (1p) model.

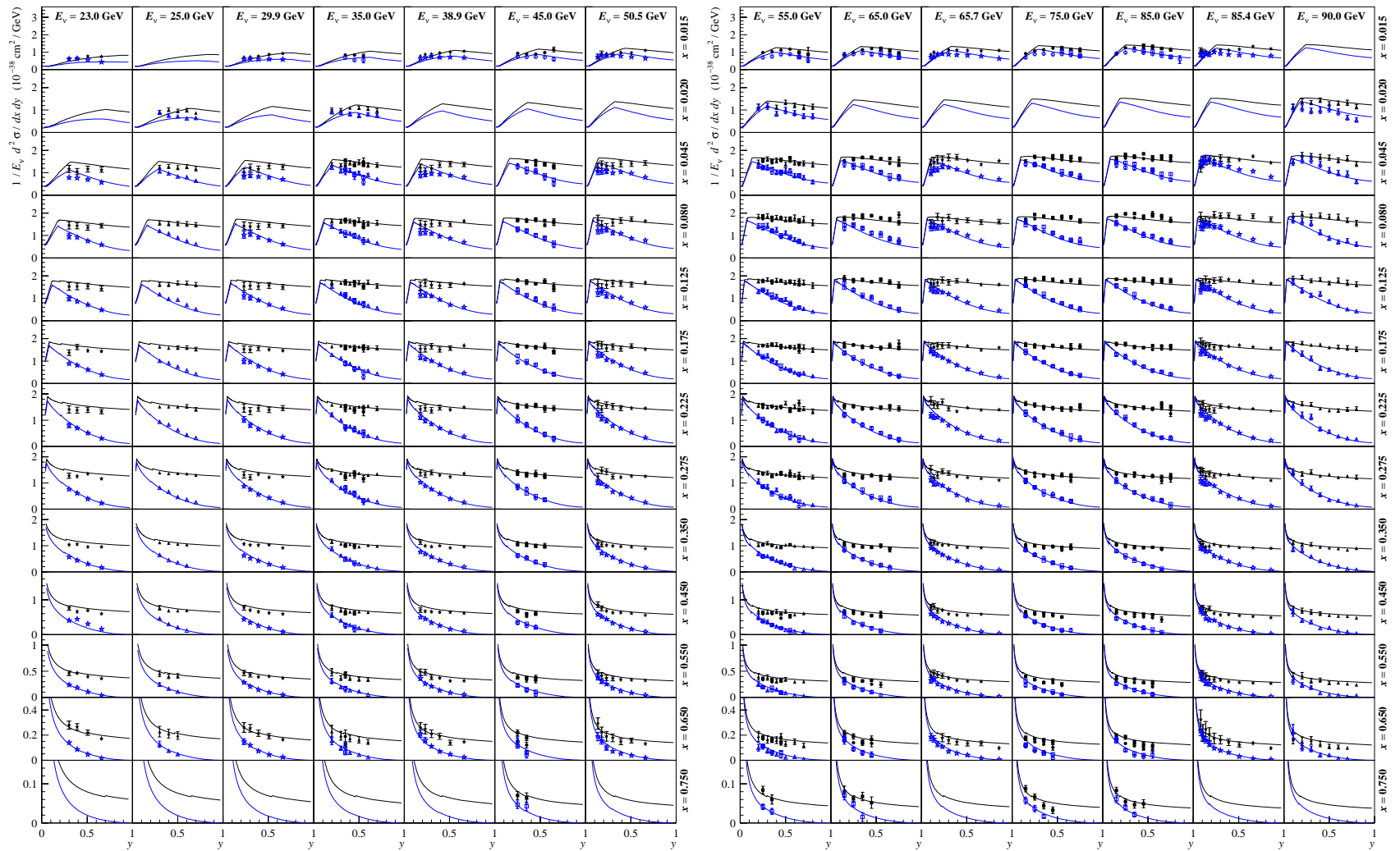
The results of experiments CDHSW 1991, CCFR 1991, and NuTeV 2005 (iron targets) and CHORUS 2006 (lead target) are shown for comparison for energies 25 to 340 GeV.

The measured cross sections are radiatively corrected and converted from the nuclear targets to a free isoscalar nucleon.

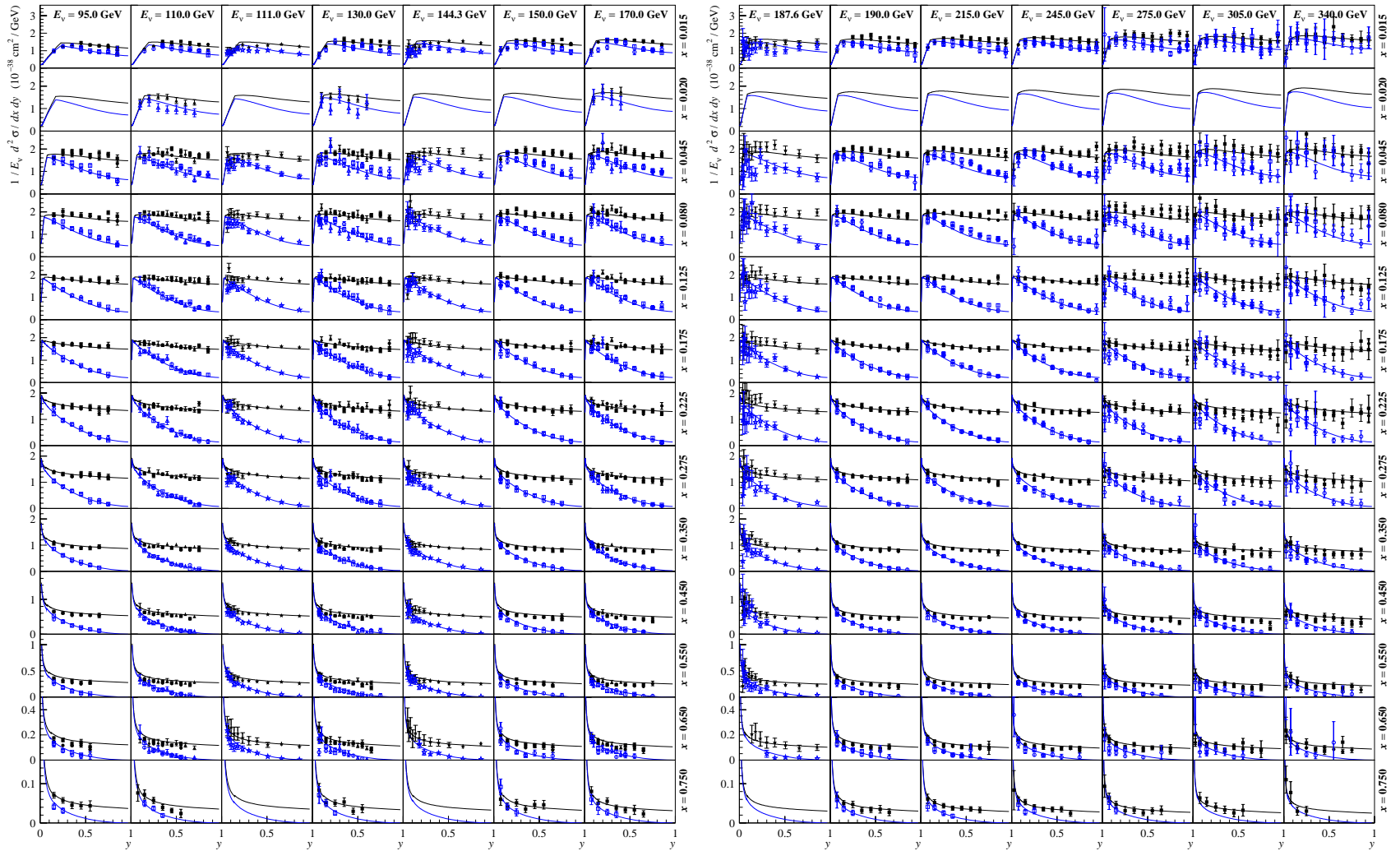
Vertical yellow lines indicate the position of the cutoff in the invariant hadronic mass:

$$W_{\text{cut}}^{\text{RES}} = W_{\text{cut}}^{\text{DIS}} = 1.44 \pm 0.02 \text{ GeV}.$$

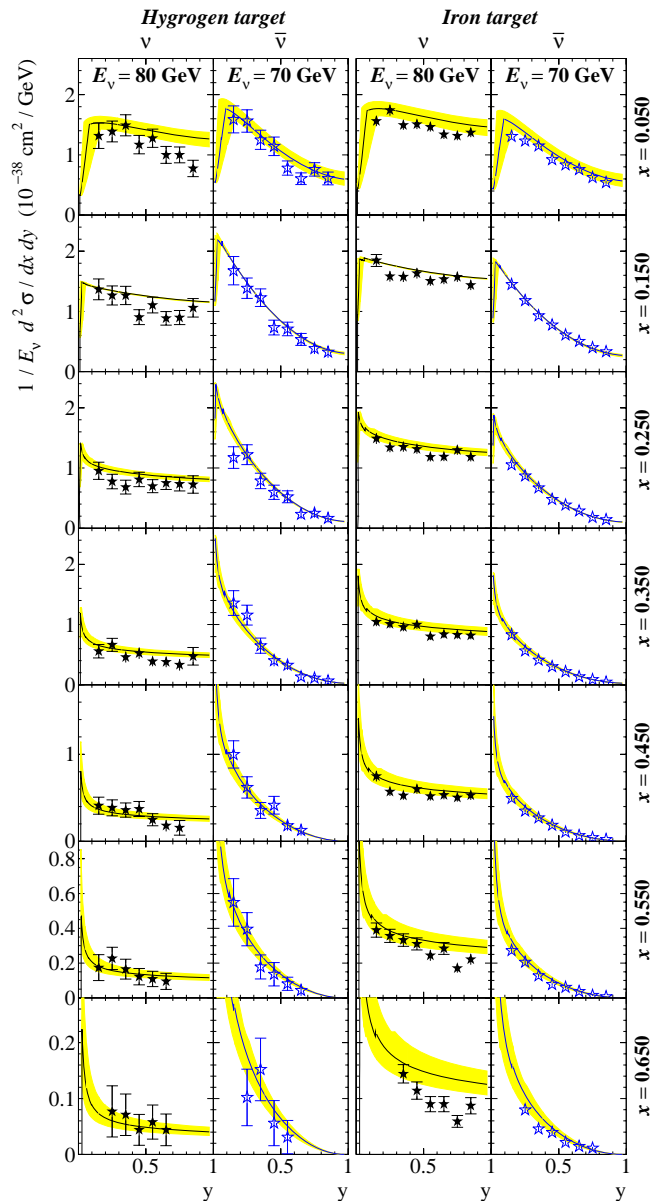
The reasons for this choice will be discussed below.



Double differential cross sections (divided by energy) for  $\nu_\mu$  and  $\bar{\nu}_\mu$  calculated using GRV 98 (1p) model in comparison with the data of CDHSW 1991, CCFR 1991, and NuTeV 2005 (iron targets) and CHORUS 2006 (lead target) for energies 23 to 90 GeV. The data is converted to a free isoscalar nucleon; radiative and nuclear corrections are included.



Double differential cross sections (divided by energy) for  $\nu_\mu$  and  $\bar{\nu}_\mu$  calculated using GRV 98 (1p) model in comparison with the data of CDHSW 1991, CCFR 1991, and NuTeV 2005 (iron targets) and CHORUS 2006 (lead target) for energies 95 to 340 GeV. The data is converted to a free isoscalar nucleon; radiative and nuclear corrections are included.



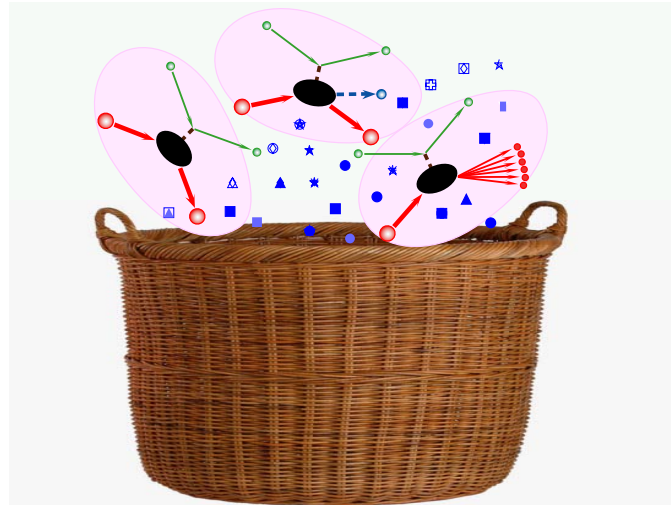
The double differential cross sections (divided by energy) for  $\nu_\mu$  and  $\bar{\nu}_\mu$  scattering off hydrogen [two left panels] and isoscalar nucleon [two right panels] vs.  $E_\nu$ ,  $x$ , and  $y$  calculated by using GRV 98 (1p) model.

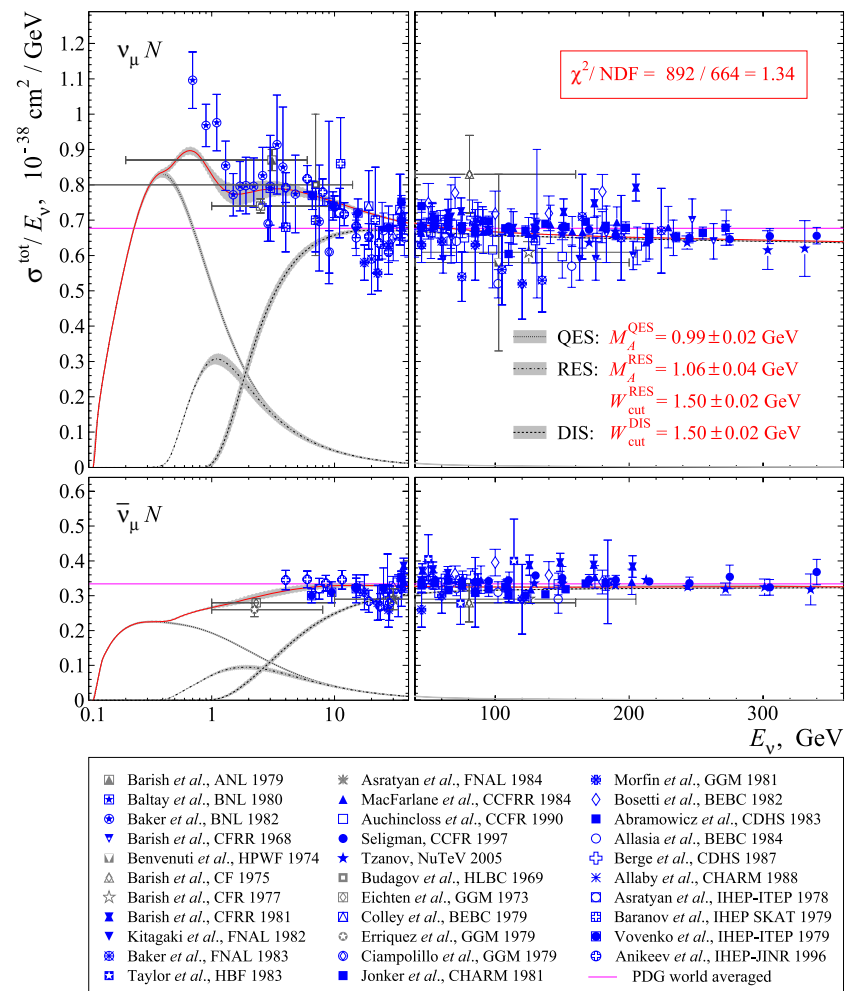
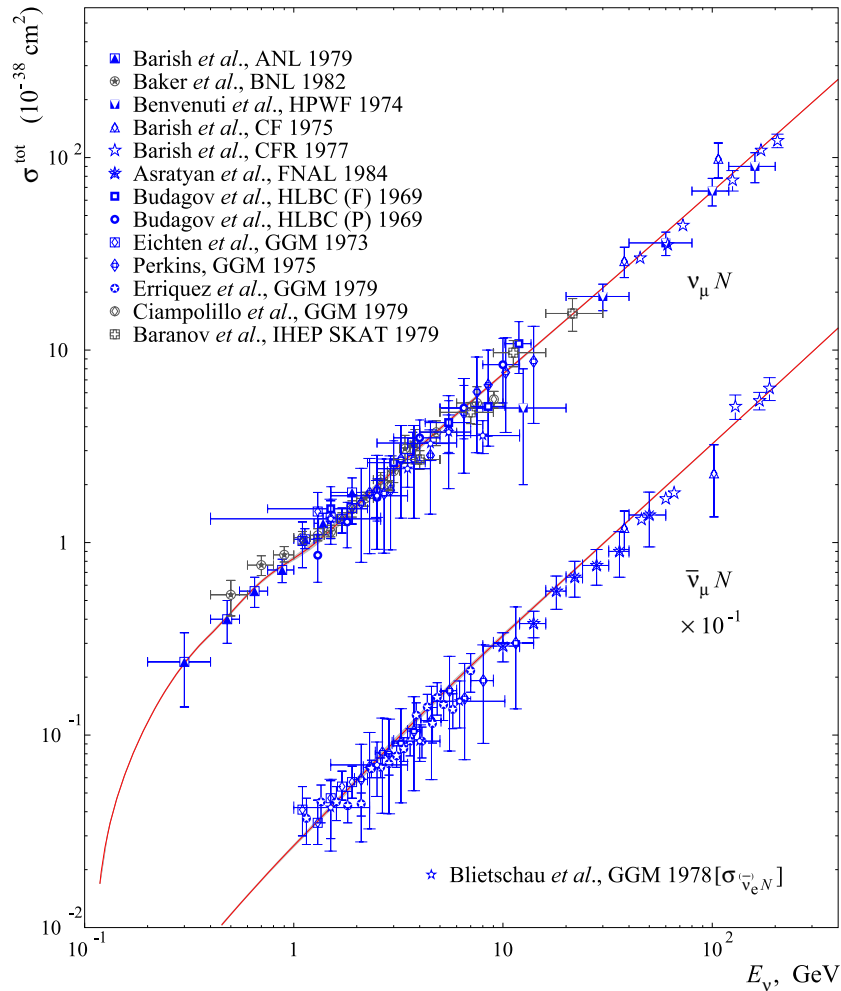
The data points are from the CDHSW 1984 experiment. The radiative corrections are included into the measured cross sections. The cross sections for iron target are converted to those for an isoscalar nucleon and nuclear corrections are added.

Yellow bands indicate the expected uncertainty due to indetermination of the incident (anti)neutrino energies (the range is  $40 < E_{\nu, \bar{\nu}} < 160 \text{ GeV}$ ), while the curves correspond to the bin centered energies  $\langle E_\nu \rangle = 80 \text{ GeV}$  and  $\langle E_{\bar{\nu}} \rangle = 70 \text{ GeV}$ .

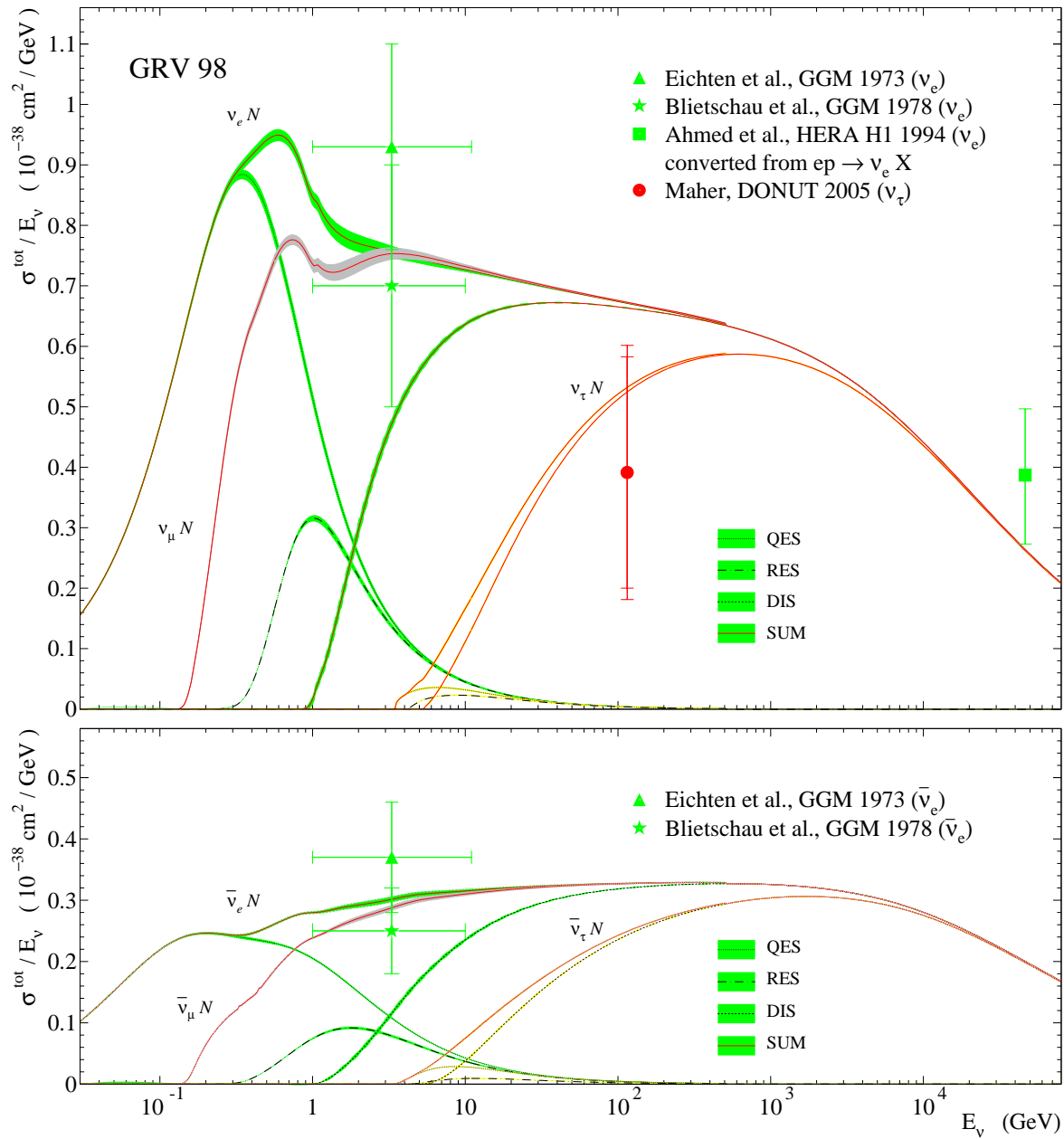
# GLOBAL FIT

(very preliminary)





Total CC cross sections and cross section slopes for  $\nu_\mu$  and  $\bar{\nu}_\mu$  scattering off an isoscalar nucleon.



Comparison of the total cross section slopes for  $\nu_e$  ( $\bar{\nu}_e$ ),  $\nu_\mu$  ( $\bar{\nu}_\mu$ ),  $\nu_\tau$  ( $\bar{\nu}_\tau$ ) scattering on isoscalar nucleon.

Also shown are the QES (both  $\Delta Y = 0$  and  $\Delta Y \neq 0$ ), RES, and DIS contributions for  $\nu_e$  ( $\bar{\nu}_e$ ) and  $\nu_\tau$  ( $\bar{\nu}_\tau$ ). The DIS contributions are calculated with GRV 98 (1p) PDFs.

The highest energy point obtained by the H1 Collaboration at HERA  $ep$  collider is a result of a (*model dependent*) conversion from the data on inverse reaction  $e^-p \rightarrow \nu_e + \text{hadrons}$ .

